The GEM Faulted Earth Subduction Interface Characterisation Project

Report produced in the context of the GEM Faulted Earth Global Component

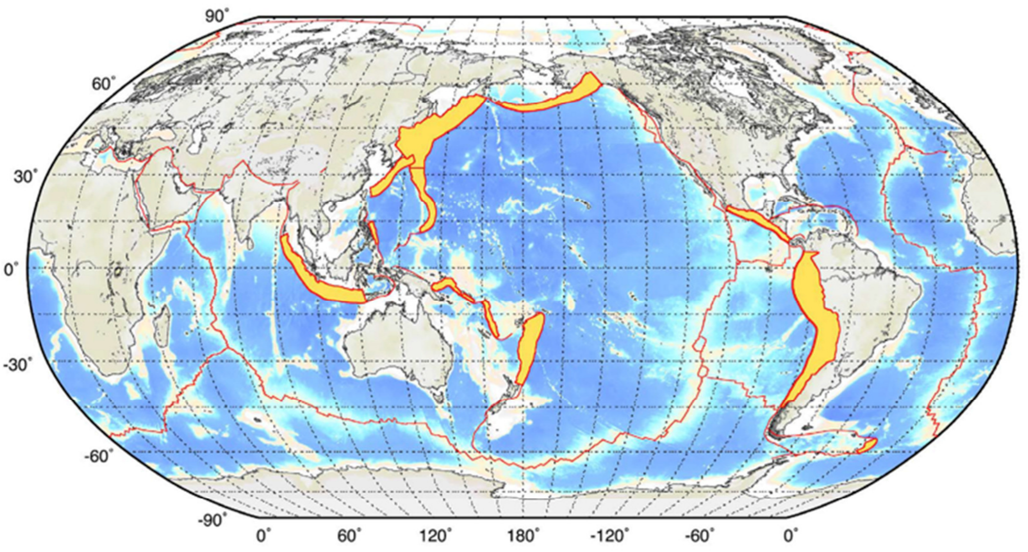

Version 2.0 – April 2015

K. Berryman[1], L. Wallace[2], G. Hayes[3], P. Bird[4], K. Wang[5], R. Basili[6], T. Lay[7], M. Pagani[8], R. Stein[3], T. Sagiya[9], C. Rubin[10], S. Barreintos[11], C. Kreemer[12], N. Litchfield[1], M. Stirling[1], K. Gledhill[1], K. Haller[3], C. Costa[13]

[1] GNS Science, New Zealand [2] University of Texas, Institute for Geophysics [3] USGS [4] UCLA [5] Canada Geological Survey [6] INGV [7] University of California Santa Cruz [8] GEM Foundation [9] Nagoya University, Japan [10] Earth Observatory, Singapore [11] University of Chile [12] University of Nevada [13] University of San Luis, Argentina

The GEM Faulted Earth Subduction Interface Characterisation Project

GEM Faulted Earth Global Component Project

Part of deliverable: 7 Completion of fault sources--subduction interfaces

Version: 2.0

K. Berryman, L. Wallace, G. Hayes, P. Bird, K. Wang, R. Basili, T. Lay, M. Pagani, R. Stein, T. Sagiya, C. Rubin, S. Barreintos, C. Kreemer, N. Litchfield, M. Stirling, K. Gledhill, K. Haller, C. Costa

April, 2015

Citation: Berryman K., Wallace L., Hayes G., Bird P., Wang K., Basili R., Lay T., Pagani M., Stein R., Sagiya T., Rubin C., Barreintos S., Kreemer C., Litchfield N., Stirling M., Gledhill K., Haller K., Costa C. (2015) The GEM Faulted Earth Subduction Interface Characterisation Project, Version 2.0, April 2015, GEM Faulted Earth Project], available from http://www.nexus.globalquakemodel.org/gem-faulted-earth/posts.

www.globalquakemodel.org

ABSTRACT

The aim of this document is to develop a globally consistent characterisation of the world's subduction interface plate boundary faults, to be used as a basis for generating earthquake event sets for inclusion in earthquake hazard and risk modelling. Given the obvious complexity of processes operating in subduction zones, and the recognition that the historical period is too short to provide a good basis for determining the frequency and maximum magnitude of earthquakes, there is a clear need to find a pragmatic approach that uses as much of the available knowledge as is possible, in a way that is neither too conservative nor too optimistic. In addition to outlining a viable approach to integrating subduction interface earthquake sources into a hazard model, we develop a comprehensive database of preferred source parameters and associated uncertainties to use for all of the world's subduction zones (see Table and Appendices). The development of these parameters is based on an extensive literature search, and via consultation among the co-authors of this report.

Keywords: subduction interface; earthquake source; source parameters; maximum magnitude

TABLE OF CONTENTS

Page

LIST OF FIGURES

LIST OF TABLES

1 Introduction

As a component of the hazard models being developed by GEM (http://www.globalquakemodel.org/) our project (http://www.globalquakemodel.org/what/global-projects/active-faults-database/) has sought to develop a globally consistent characterisation of the world's approximately 55,000 km of subduction interfaces as a basis for generating earthquake event sets for inclusion in earthquake hazard and risk modelling.

Subduction zones are where the majority of global seismic energy is released and, because of their dimensions, are where the largest and some of the most damaging earthquakes and associated tsunami have occurred. Recent examples include the Mw 9.2, December 26th, 2004 Sumatra earthquake and the Mw 9.0, March 11th, 2011 Tohoku earthquake. Thus, to underpin a global earthquake risk assessment, characterisation of subduction zones are crucial ingredients.

In December 2011 an invited group of scientists (the report authors) with extensive knowledge of subduction zones around the world met for four days to discuss the approach we should take to compile a database and also to begin populating the attributes of the 40 subduction zones identified (Figure 1). The process of attribution and discussion has continued to June 2014, refining the parameters and uncertainties. Note that the segments defined are not intended to represent rupture segments. They are largely chosen where plate motion rate or azimuth of subduction undergoes a change, or where there is a change in the plate pairs that are juxtaposed at the boundary. Where the segments link-up geometrically the possibility of multi-segment rupture must be included in the hazard model.

There is a rich scientific legacy of work on subduction zones globally, and a wealth of historical data to draw on, but the 2004 Sumatra earthquake, and more recently the Tohoku earthquake, have surprised many researchers in terms of the size of the event (see McCaffrey, 2008 for recent review). Many investigators have attempted to explain subduction seismogenesis by correlating the frequency and magnitude of earthquakes with geodynamic parameters, such as subduction rate, subducting plate age, subduction interface thermal structure, or the presence of subducting sediment (e.g., Uyeda and Kanamori, 1979; Ruff and Kanamori, 1980; Peterson and Seno, 1984; Kanamori, 1986; Ruff, 1989; Scholz and Campos, 1995, 2012; McCaffrey, 1997). However, recent large earthquakes, and further research, question the utility of some of the correlations as proxies for seismogenesis (e.g., Subarya et al., 2006; Stein and Okal, 2007; McCaffrey, 2008). In the Hikurangi subduction zone of New Zealand, Wallace et al. (2009b) suggest that there is a complex interplay between upper and lower plate structure, subducting sediment, thermal effects, regional tectonic stress regime, and fluid pressures, and all of these factors probably control the extent, and thus the possible maximum magnitude of subduction thrust earthquakes. In the Japan region there have been great earthquakes in both the northeast where the incoming plate is old and the rate of subduction is fast (>80 mm/a) and in the southwest where the plate is young and the rate is only half of that in the northeast.

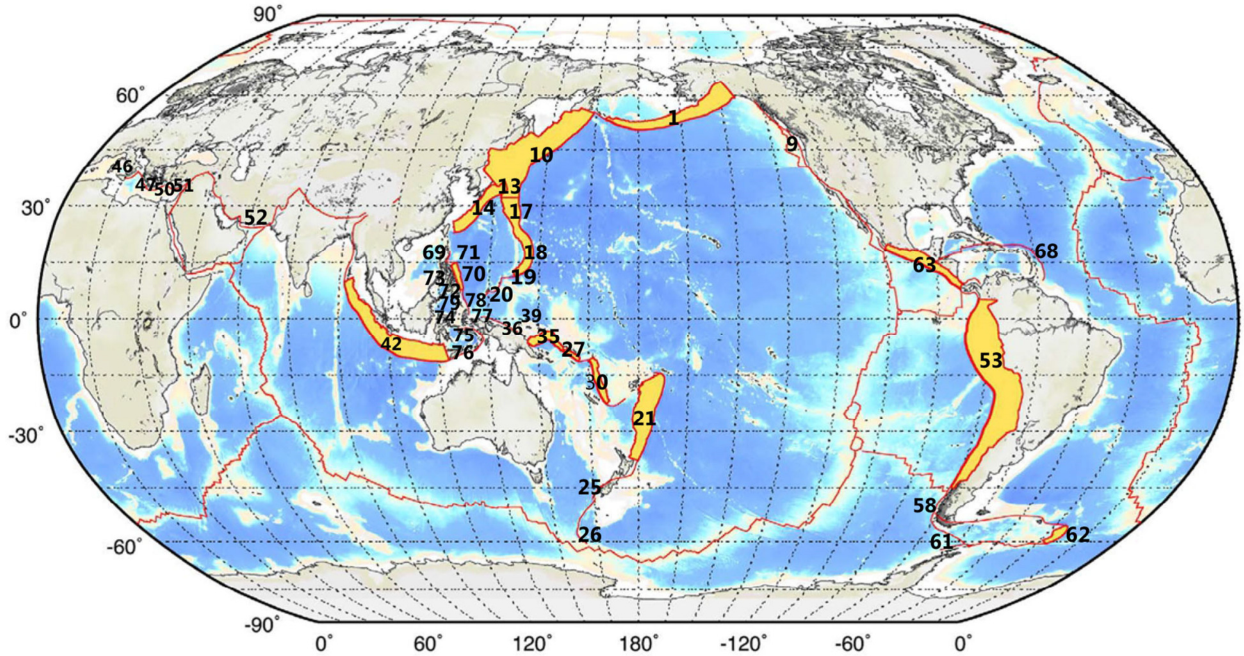

Figure 1.1 Location of the subduction zones identified in this database modified from Hayes et al. (2012) reproduced with permission of John Wiley and Sons. This is Figure 1 in the paper, Slab1.0: A three-dimensional model of global subduction zone geometries' by Hayes, Wald and Johnson published in the Journal of Geophysical Research, Volume 117, B01302, Copyright 2012. Several subduction zones are divided into segments. Therefore, the subduction zone labels are not sequential, and correspond with the listing in Table 3.1.

Given the obvious complexity of processes operating in subduction zones, and the recognition that the historical period is too short to provide a good basis for determining the frequency and maximum magnitude of earthquakes in any, let alone all of the Earth's subduction zones, there is a clear need to find a pragmatic approach that uses as much of the available knowledge as is possible, in a way that is neither too conservative nor too optimistic. The tools and techniques that we have used include improved understanding of the geometry of most of the global subduction zones via the SLAB1.0 model (Hayes et al., 2012), plate motions incorporating upper plate rotations and backarc motions (e.g., Bird, 2003; Bird et al., 2009), historical event catalogues (e.g., Heuret et al., 2011), increasingly robust plate models built from GPS velocities (e.g., DeMets et al., 2010), and the widely used, but nevertheless debated methods of earthquake hazard assessment (e.g., Stein et al., 2012; Hanks et al., 2012).

In this report we assess the parameters associated with the plate interface itself and do not include seismicity within the down-going plate or overriding plate. To accurately estimate the total hazard associated with subduction zones, one also needs to consider plate-bending earthquakes and earthquakes associated with deformation of the down-going plate before it enters the subduction zone – so-called 'outer rise' events, as well as events occurring in the upper plate. These are outside of the scope of this report. In characterising the subduction interface we adopt some aspects of the approach presented by McCaffrey (2008), including a procedure for prescribing length-limited estimates of maximum magnitude. In the absence of adequately long records of earthquakes for most subduction zones, and the occurrence of unexpectedly large and long ruptures in Indonesia and Japan, we conclude that earthquake magnitude is probably only limited by available subduction length. The approach presented here provides a basis for developing earthquake event sets for the subduction zones of the World on a consistent basis using an up-to-date synthesis of available published data. We assign the maximum magnitude to each subduction zone based on its total length. If the total length of the subduction zone exceeds what can realistically rupture with the generally accepted maximum magnitude of Mw 9.6 then we propose that the earthquake events should ‘float’ along the whole subduction zone, using the available seismic moment respecting the maximum magnitude and the Gutenberg and Richter b value, in the manner developed by Parsons et al. (2012) for the Nankai Trench in Japan. The key, and perhaps most contentious assumption in this approach is that any subduction zone may rupture a surprisingly long segment along strike regardless of its geological conditions, but the recurrence time of such events will vary dramatically between subduction zones according to those geological conditions. A recent example of a subduction event rupturing through what had previously been considered a segment boundary is the 2007 Mw 8.1 earthquake on the Solomon Islands subduction zone (Taylor et al., 2008a). The recurrence time for all earthquakes in the subduction zone further depends on the fraction of the plate motion convergence rate that is released as earthquakes, the so-called coupling coefficient. A very conservative treatment is to assume all relative plate motion is converted to seismic moment release (i.e., 100% coupling) but observations have shown this to be an unlikely end-member model. The initial assessment of subduction zones into “Chilean type” and “Mariana type” (Uyeda & Kanamori, 1979) still demonstrates some first-order coherence in terms of variations in seismic coupling among subduction zones. Together with other data, particularly the interpretation of campaign and continuous GPS velocities (see Appendix B), these observations provide a basis for assessments of seismic coupling that ranges from near to 90% in Cascadia and Nankai to as low as 15% at the Manila trench. Despite this low coupling in subduction zones like the Manila Trench, following the assumption of McCaffrey (2008), very large events can still occur there because the subduction zone is sufficiently long. What makes the short-term hazard low at the Manila trench is the extremely long recurrence time of full-margin rupture.

Determination of the Gutenberg & Richter b-value (the long-term ratio of small to large events that comprise the co-seismic component of plate motion measured over the duration of a seismic cycle) is a key requisite for calculating hazard. The b-value is an important driver of seismicity rate calculations, and seemingly small changes to the b-value can result in significant differences in hazard estimates, an observation directly attributable to the log-linear relationship between frequency and magnitude. For example, a distributed seismicity source model with a b-value range of 0.6 to 1.0 (all else held constant) produces hazard estimates (e.g., peak ground accelerations) that vary by about 30%. In continental settings the b-value is observed to fall in the range of about 0.6 to 1.5. Bird and Kagan (2004) deduced a global average subduction b-value of 0.96 with a 95% confidence interval of 0.90 to 1.02, but this includes plate-bending earthquakes in the downgoing plate as well as interface events. Suckale and Grünthal (2009) reported a lower b-value of 0.71 from historical events in the New Hebrides region. On closer inspection the historic events upon which these assessments have been made should more correctly be termed b-values from the subduction zone region, as they often include only sparse events from the locked part of the interface, as well as crustal and plate-bending events in the downgoing plate. Thus, for characterising likely future major events on the locked part of the interface these studies may not be the most appropriate.

A long record of large interface events has been obtained by Goldfinger et al. (2012) using paleoseismic methods in the Cascadia margin of western North America. Studies in this region suggest a paucity of moderate magnitude events in this region but the data are almost certainly incomplete. Nevertheless it appears that some subduction zones are highly productive while others are “quiet” suggesting that much of the available seismic moment on the locked part of the interface is released in infrequent large events. At these margins the b-value is likely to be lower over complete seismic cycles than for productive regions such as the New Hebrides. Heuret et al. (2011) examined seismicity rates specifically on the thrust interface of subduction zones (Figure 2) and identified low rates of ≥Mw 5.5 events on the Hikurangi, Caribbean, southern Chile, western and eastern Aleutians, Java, and the Makran interface zones. For these unproductive zones the b-value is likely to be substantially lower than the global average b-value which has been obtained from locations where there has been significant activity in the instrumental period. Conversely, Heuret et al. (2011) also identify some margins where the rate of interface events of ≥Mw 5.5 is high which are those regions where the 'global average' of Bird and Kagan (2004) is likely to be representative.

To further illustrate likely variability in b-values at subduction zones, we have compiled a list of published b-values (Table 3.2). At individual subduction zones (such as the Tonga Trench), estimated b-values can vary by as much as 0.5 or more between studies. The lowest b-values in Table 3.2 are ~0.6 (New Hebrides, Solomon Islands), while the highest ones are ~1.5 (Marianas). To encompass this uncertainty, we assume a minimum b-value for all subduction zones of 0.7, and a maximum of 1.2. In cases where published studies have estimated b-values that are less than 0.7, or exceed 1.2, we use the published values to inform the minimum or maximum value in our table. In addition to these three principal parameters of seismogenesis – maximum magnitude, seismic coupling coefficient, and b-value – we also need to define the potential upper and lower extent of rupture in future interface earthquakes to position the rupture plane with respect to the land surface above, as input to hazard and risk calculations.

When implemented in a seismic hazard model, the procedure should be to generate earthquakes of appropriate size and frequency within a subduction zone that uses the available seismic moment as defined for that region. Here, we define the maximum magnitude for each subduction zone, and the moment from earthquakes in a seismic hazard model should be balanced over the entire fault surface, similar to that proposed for the fault slip component of a California hazard model developed by Hiemer et al. (2013), and by the 'earthquake simulator developed by Parsons et al. (2012) for the Nanakai subduction zone.

In the database we constrain lower bound maximum magnitudes in each subduction segment as the largest earthquake that has occurred in the instrumental record as defined in most recent literature. In some places, such as for the 1960 rupture in Chile this may narrow the range of Mmax because the 1960 Mw 9.5 is close to the theoretical maximum magnitude proposed by McCaffrey (2008) of Mw 9.6. Where no great earthquakes (Mw > 8) have occurred in the instrumental period the range applied to Mmax is often at least one magnitude unit. By capturing some estimate of uncertainty in many of the key parameters the database lends itself to creating alternate event sets for each subduction segment via Monte Carlo sampling, and for frequent updating as new data come to hand.

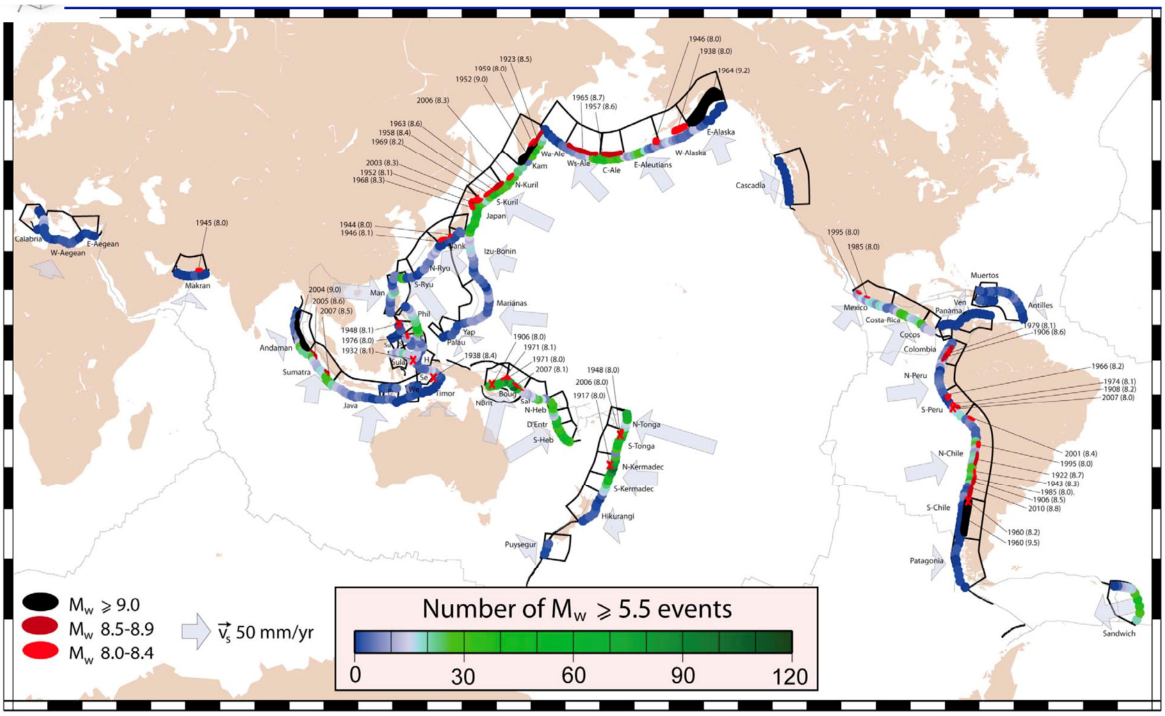

Figure 1.2 Subduction zone interface seismicity and trench segmentation, from Heuret et al. (2011) reproduced with permission of John Wiley and Sons. This is Figure 1 in the paper 'Physical characteristics of subduction interface type seismogenic zones revisited' by Heuret, Lallemand, Funiciello, Piromallo and Faccenna published in Geochemistry, Geophysics, Geosystems 12: Q01004, Copyright 2011. The figure and part of the following caption are reproduced with permission of John Wiley & Sons. The rupture area of the Mw ≥ 8.0 subduction interface events (1900–2007) is represented by red and black ellipses. The rupture areas were taken from McCann et al. (1979), Kanamori (1986), Schwartz et al. (1989), Byrne et al. (1992), Tichelaar and Ruff (1993), Johnson et al. (1994), Ishii et al. (2005), Fedotov et al. (2007), Ruppert et al. (2007), Bilek (2010), and Madariaga et al. (2010). Red crosses are used here to indicate Mw ≥ 8.0 events that did not have available rupture area data. Colored dots represent, by each 1° of trench, the number of Mw ≥ 5.5 subduction interface events (1976–2007). Subduction velocities (Heuret, 2005) are represented by blue arrows, although in this study we use velocities from more recent geodetic studies (see Appendix B) and Bird (2003), rather than the ones shown here. In this study we relax the segmentation model delimited by Heuret et al. (as black lines in this figure), and propose to 'float' earthquakes along the whole subduction zone as discussed in the text.

2 Procedure

To populate the database we have firstly defined subduction zones, and in some cases segments, where there is a change in kinematics at the subduction zone (usually due to the juxtaposition of different plate pairs and/or major changes in plate boundary orientation). These segments are largely defined for kinematic convenience when calculating the plate rates at the segment endpoints, but in some cases these segments represent possible rupture segments (as in the Alaska case; Wesson et al., 2007). In the database, we record the plate pairs at each subduction segment, define the segment coordinate endpoints, the average dip of the seismogenic portion of the interface, the dip direction, and the trench depth. Most of these values are inferred from observations. The down-dip geometry of subduction zones are those identified in the SLAB 1.0 model of Hayes et al. (2012) which is available on-line from US Geological Survey (see: http://earthquake.usgs.gov/data/slab/). The geometry of zones in Slab 1.0 is determined from careful examination of instrumental seismicity. In subduction zones where there is little seismicity this basis for defining geometry is not available and so we have assigned estimates of dip angle from the literature. Uncertainty in the dip angle could also be incorporated into the estimate of fault area and maximum magnitude, but for this study we consider this to be relatively well constrained and uncertainty will have a relatively small impact on hazard compared with uncertainty in coupling coefficients and b-values.

Important judgments are then made for the maximum up-dip extent of ruptures, including uncertainty estimates (min, preferred, max), and the down-dip extent of ruptures, again with uncertainty (min, preferred, max). The down-dip rupture width can then be calculated. Another parameter requiring considerable judgement is the coupling coefficient in the particular subduction segment and again we assign uncertainty (min, preferred, max). We outline the rationale behind our choice of coupling coefficients for each subduction zone in Appendix B. For all segments, we assume a range of Mmax values, with the largest possible Mmax based on rupture length of the entire segment (or combination of segments), using scaling relationships between subduction zone (or segment) length and magnitude in McCaffrey (2008). The minimum Mmax value is taken as the largest earthquake observed in the historical record on that segment. As a default for the preferred value, we take the average of the minimum and maximum Mmax values. The b-value for the subduction zone is also a significant judgement as discussed above, and so considerable uncertainty is applied to this parameter also.

With all of these parameters defined or calculated, a series of earthquake event sets can then be calculated for each subduction segment defining the frequency-magnitude distribution and the recurrence of each earthquake. Monte Carlo sampling of the range of event sets can determine uncertainty statistics for each event set.

3 Results

A wide range of possible earthquakes have been identified in this project, reflecting widely varying parameters (Table 3.1). Subduction segment lengths range from as little as 229 km (Halmahera segment in the Molucca Sea) to 6536 km for the South American margin. The dip on the seismogenic interface ranges from 6° in the Prince William Sound segment of the Alaska subduction zone to 28° in a segment of the New Hebrides subduction zone. The up-dip extent of rupture is often thought to be 5-10 km below the seafloor, although in many places the possibility of rupture to the trench is given some weight. The down-dip limit of rupture is also expected to vary significantly – as shallow as 15 km in the Yakataga segment of Alaska or as deep as 50 km in Japan and Chile. With these wide ranges of dip and rupture limits, the rupture widths vary from as little as 40 km in the Yakataga segment of Alaska and parts of the New Hebrides region, to as much as 240 km in the shallowly-dipping Prince William Sound segment of the Alaska subduction margin.

The wide range of segment lengths and widths is responsible for the range of maximum earthquake magnitudes expected in global subduction zones (Figure 3.1). The preferred maximum magnitude earthquakes expected in the Hjort (south of New Zealand), Calabria, and east Luzon subduction zones are only Mw 7.8, and, while at the other end of the spectrum a Mw 9.5 is the calculated preferred estimate for central Chile, and in several subduction zones the available length in the subduction zone cannot preclude the occurrence of the generally accepted global maximum Mw 9.6 event. Accepting uncertainties in the estimated parameters, and in delineation of segments of subduction zones, we find that maximum magnitude earthquakes of Mw 9.6 appear possible in 10 of the 79 subduction zones or their segments as defined in this project, and a maximum of Mw 9.0 to 9.5 is possible in an additional 36 of the 79 subduction zones or their segments (Table 3.1).

Figure 3.1 shows that there is a clear positive correlation between magnitude and area (R=0.81), and a weaker but positive correlation between magnitude and coupling coefficient (R=0.51) (red and orange symbols tend to sit above blue symbols). There appears to be a weaker or no correlation (R=0.28) between maximum magnitude and average velocity across the plate interface (larger symbols tend to fall in the lower magnitude and lower area quadrants of the plot). Similarly, there is poor correlation between coupling coefficient and area (R=0.27). The correlation between magnitude and area is expected because magnitude is derived in large part from the area. A positive correlation between coupling coefficient and magnitude can be understood as larger locked patches on the fault plane resulting in larger earthquakes. The finding that relative plate velocity is poorly correlated with magnitude is somewhat surprising, but it may be that higher velocities result in more fracturing and break-up of the down-going plate and therefore smaller area of locked patches. Higher velocities could also lead to less fault healing and hence lower coupling.

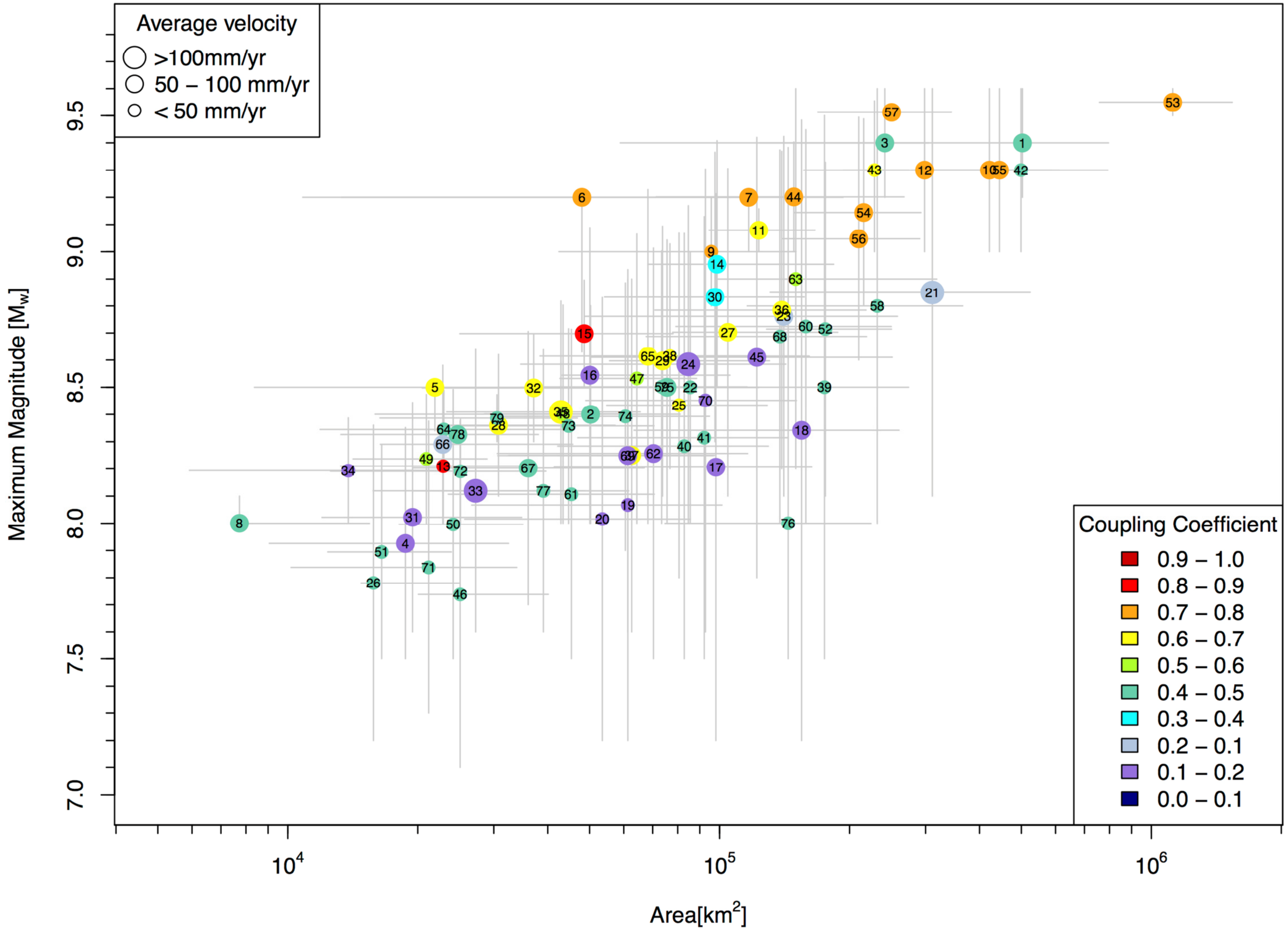

Figure 3.1 Plot showing relationships between maximum magnitude, rupture area, coupling coefficient and relative velocity across the interface for each of the 79 subduction interface zones and their possible segments considered in this study.

Table 3.1 Subduction Interface Zone Parameters as defined in Appendix A.

*Note all subduction zones divided into segments (Alaska, Central America, much of the South American margin) are considered to be plausible segments based on trench geometry and kinematics. However, an alternative and recommended treatment of these very long subduction zones is to define a maximum magnitude and allow earthquakes to 'float' along the total length with the earthquake event set determined by plate convergence rates, coupling coefficient and b-value of the interface source zone. The abbreviated names of the overriding/subducting plates follow those defined in Bird (2003) (see table 1 in that publication).

No.	Subduction Zone	Segment	Plate pairs	Left_E_LONG	Left_N_LAT	Left_REL_VEL (mm/yr)	Left_REL_AZI (°)	Right_E_LONG	Right_N_LAT	Right_REL_VEL (mm/yr)	Right_REL_AZI (°)	Length (km)
1	**Alaska/ Aleutians**	**Whole margin**	**PA\NA**	**164.066**	**55.209**	**74.6**	**311**	**-140.128**	**60.381**	**49.0**	**350**	**4130**
2	Alaska	Komandorski	PA\NA	164.066	55.209	74.6	311	170.700	52.498	74.3	313	531
3	Alaska	Western Aleutians	PA\NA	170.700	52.498	74.3	313	-162.413	53.367	64.0	329	1963
4	Alaska	Shumagin	PA\NA	-162.413	53.367	64.0	329	-157.986	54.101	61.0	332	302
5	Alaska	Semidi	PA\NA	-157.986	54.101	61.0	332	-154.160	55.239	58.4	336	279
6	Alaska	Kodiak	PA\NA	-154.160	55.239	58.4	336	-149.220	56.925	55.0	340	361
7	Alaska	Prince William Sound	PA\NA	-149.220	56.925	55.0	340	-144.316	59.918	51.4	347	444
8	Alaska	Yakataga	PA\NA	-144.316	59.918	51.4	347	-140.128	60.381	49.0	350	250
9	**Cascadia**		JF\NA	-130.850	51.612	47.8	58	-124.742	40.313	32.7	58	1415
10	**Japan/Kurile**	**Whole margin**	**PA\OK**	**141.992**	**34.666**	**93.0**	**294**	**164.066**	**55.209**	**78.7**	**308**	**2965**
11	Japan/Kurile	Japan Trench	PA\OK	141.992	34.666	93.0	294	144.454	40.847	91.1	295	742
12	Japan/Kurile	Kurile-Kamchatka	PA\OK	144.454	40.847	90.9	296	164.066	55.209	78.7	308	2223
13	**Kanto**		PS\OK	138.674	35.034	36.0	317	141.883	34.213	34.1	312	312
14	**Nankai/Ryukyu**	**Whole margin**	**PS\AM, PS\ON**	**122.501**	**23.643**	**134.0**	**314**	**138.674**	**35.034**	**44.4**	**310**	**2202**
15	Nankai/Ryukyu	Nankai	PS\AM	132.824	30.754	55.7	310	138.674	35.034	44.4	310	762

No.	Subduction Zone	Segment	Plate pairs	Left_E_LONG	Left_N_LAT	Left_REL_VEL (mm/yr)	Left_REL_AZI (°)	Right_E_LONG	Right_N_LAT	Right_REL_VEL (mm/yr)	Right_REL_AZI (°)	Length (km)
16	Nankai/Ryukyu	Ryukyu	PS\ON	122.501	23.643	134.0	314	132.824	30.754	58.0	311	1440
17	**Izu-Bonin**		PA\PS	143.522	24.391	47.1	292	141.883	34.213	61.4	284	1128
18	**Marianas**		PA\MA	143.503	11.494	76.3	277	143.522	24.391	49.1	281	1822
19	**North Yap**		PA\PS	138.359	9.379	3.0	297	143.097	11.569	9.0	311	690
20	**Palau-South Yap**		CL\PS	134.521	6.990	1.6	318	138.359	9.379	7.1	324	554
21	**Hikurangi-Tonga-Kermadec**	**Whole margin**	**PA\HF, KE,TO**	**175.503**	**-42.059**	**19.5**	**236**	**-173.407**	**-14.584**	**269.5**	**256**	**3412**
22	H-T-K	Hikurangi	PA\HF	175.503	-42.059	19.5	236	179.838	-37.476	65.5	247	660
23	H-T-K	Kermadec	PA\KE	179.838	-37.476	45.3	258	-174.985	-23.750	98.1	257	1627
24	H-T-K	Tonga	PA\TO	-174.985	-23.750	112.6	248	-173.407	-14.584	269.5	256	1125
25	**Puysegur**		AU\PA	168.770	-44.021	36.6	68	163.235	-50.079	29.9	51	834
26	**Hjort**		see notes	157.615	-57.474	25.2	19	161.228	-61.457	18.9	342	493
27	**Solomons**	**Whole margin**	**WL\PA, AU\PA**	**153.083**	**-5.750**	**91.1**	**49**	**164.612**	**-10.892**	**88.4**	**80**	**1460**
28	Solomons	Northwest	WL\PA	153.083	-5.750	91.1	49	156.296	-8.174	107.0	47	465
29	Solomons	Southeast	AU\PA	156.296	-8.174	98.1	75	164.612	-10.892	88.4	80	995
30	**New Hebrides**	**Whole margin**	**AU\PA, NH,MH**	**164.612**	**-10.892**	**94.7**	**78**	**174.277**	**-22.667**	**45.8**	**7**	**1923**
31	New Hebrides	North	AU\PA	164.612	-10.892	94.7	78	166.106	-13.634	90.7	79	400
32	New Hebrides	Central	AU\NH	166.106	-13.634	33.7	74	167.350	-18.022	102.3	74	500
33	New Hebrides	South	AU\NH	167.350	-18.022	102.3	74	169.954	-22.325	174.9	68	560
34	New Hebrides	Matthew-Hunter	AU\MH	169.954	-22.325	49.1	8	174.277	-22.667	45.8	7	463
35	**New Britain**		WL\SB	147.283	-7.000	48.7	21	153.083	-5.750	160.0	-3	660

No.	Subduction Zone	Segment	Plate pairs	Left_E_ LONG	Left_N_L AT	Left_REL_V EL (mm/yr)	Left_REL _AZI (°)	Right_E_ LONG	Right_N_ LAT	Right_REL _VEL (mm/yr)	Right_REL_ AZI (°)	Length (km)
36	**New Guinea Trench**	**Whole margin**	**PA\NGH, CL\BH**	**143.743**	**-3.200**	**92.6**	**251**	**132.515**	**0.017**	**22.1**	**183**	**1364**
37	NGT	east	PA\NGH	143.743	-3.200	92.6	251	138.793	-1.159	84.1	259	600
38	NGT	west	CL\BH	138.793	-1.159	28.1	185	132.515	0.017	22.1	183	764
39	**Manus Trench**	**Whole margin**	**PA,CL\NB**	**154.955**	**-4.550**	**10.0**	**181**	**142.246**	**-2.693**	**8.7**	**141**	**1709**
40	Manus	East	PA\NB	154.955	-4.550	10.0	181	149.270	-0.650	6.9	162	809
41	Manus	West	CL\NB	149.270	-0.650	16.9	152	142.246	-2.693	8.7	141	900
42	**Sunda Trench**	**Whole margin**	**AU\BU,SU**	**92.068**	**13.715**	**12.4**	**178**	**120.886**	**-11.493**	**69.3**	**8**	**4874**
43	An-Sunda Tr.	Andaman	IN or AU\BU	92.068	13.715	12.4	178	96.202	1.345	50.8	90	1579
44	An-Sunda Tr.	Sumatra	AU\SU	96.202	1.345	46.4	1	104.576	-8.167	55.7	11	1438
45	An-Sunda Tr.	Java	AU\SU	104.576	-8.167	55.7	11	120.886	-11.493	69.3	8	1857
46	**Calabria**		AF\EU	15.775	37.282	2.0	306	17.415	39.071	2.0	306	245
47	**Hellenic Trench**	**Whole margin**	**AF\AS**	**19.912**	**37.731**	**23.0**	**26**	**28.726**	**36.579**	**10.0**	**37**	**1032**
48	Hellenic Tr.	western segment	AF\AS	19.912	37.731	23.0	26	25.288	34.202	35.0	35	620
49	Hellenic Tr.	eastern segment	AF\AS	25.228	34.202	10.0	37	28.726	36.579	10.0	37	412
50	**Cyprus**	western segment	AF\AT	28.726	36.579	14.0	30	32.254	34.729	9.0	30	380
51	**Cyprus**	eastern segment	AF\AT	32.160	34.604	7.0	40	35.169	34.824	7.0	40	276
52	**Makran**		AR\EU	57.057	26.049	19.5	14	65.028	24.382	19.5	17	941
53	**South America**	**Whole margin**	**NZ\SA,ND**	**-78.646**	**7.337**	**53.0**	**80**	**-76.006**	**-45.659**	**78.7**	**80**	**6526**
54	S. America	Ecuador-Colombia	NZ\ND	-78.646	7.337	53.0	80	-81.599	-3.245	60.9	83	1329
55	S. America	Peru	NZ\SA or AP	-81.599	-3.245	70.0	82	-71.307	-21.965	63.9	78	2502
56	S. America	North Chile	NZ\SA	-71.307	-21.965	79.5	77	-73.246	-34.290	80.5	78	1394
57	S. America	Central Chile	NZ\SA	-73.246	-34.290	80.5	78	-76.006	-45.659	78.7	80	1301

No.	Subduction Zone	Segment	Plate pairs	Left_E_LONG	Left_N_LAT	Left_REL_VEL (mm/yr)	Left_REL_AZI (°)	Right_E_LONG	Right_N_LAT	Right_REL_VEL (mm/yr)	Right_REL_AZI (°)	Length (km)
58	**Patagonia**	**Whole margin**	**AN\SA,SC**	**-76.006**	**-45.659**	**21.3**	**93**	**-56.925**	**-60.565**	**10.8**	**94**	**2308**
59	Patagonia	N. Patagonia	AN\SA	-76.006	-45.659	21.3	93	-76.483	-52.068	19.3	93	731
60	Patagonia	S. Patagonia	AN\SC	-76.483	-52.068	15.1	85	-56.925	-60.565	10.8	94	1577
61	**South Shetland**		AN\SL	-56.925	-60.565	10.0	150	-63.969	-62.422	10.0	156	435
62	**South Sandwich**		SA\SW	-26.071	-60.391	84.1	262	-28.647	-55.005	66.3	266	791
63	**Mexico/Central America**	**Whole margin**	**RI,CO\NA,CA,PM**	**-106.890**	**21.799**	**13.6**	**21**	**-82.875**	**7.366**	**79.1**	**29**	**3185**
64	Mexico/CA	Jalisco	RI\NA	-106.890	21.799	13.6	21	-105.247	18.762	36.3	50	396
65	Mexico/CA	Michoacan-Guatemala	CO\NA	-105.247	18.762	44.0	36	-90.898	12.584	78.8	33	1710
66	Mexico/CA	El Salvador-Nicaragua	CO\CA	-90.898	12.584	71.3	21	-86.648	10.235	80.0	23	546
67	Mexico/CA	Costa Rica-west Panama	CO\PM	-86.648	10.235	70.8	27	-82.875	7.366	79.1	29	533
68	**Antilles**		SA or NA\CA	-58.157	10.160	20.1	263	-63.360	19.691	17.0	263	1400
69	**Manila**		SU\PS	120.452	21.632	92.0	118	119.255	16.556	97.8	116	610
70	**Philippine Trench**		**see notes**	129.197	1.059	43.0	255	124.891	14.704	29.4	256	1633
71	**East Luzon Trough**		**see notes**	122.263	15.633	14.2	257	123.483	18.067	11.9	247	290
72	**Cotabato Trench**		**see notes**	123.500	7.000	18.8	76	125.150	5.600	18.2	78	250
73	**Sulu Trench**		**see notes**	122.500	8.660	18.9	72	119.607	6.333	19.4	76	445
74	**Minahassa Trench**		**see notes**	123.430	2.006	19.1	184	119.249	0.714	51.6	170	591
75	**Seram Trough**		BH\BS	132.717	-4.440	74.2	257	126.167	-2.750	66.1	267	815
76	**Timor**		BS\TI	132.689	-6.681	23.4	132	120.543	-7.812	35.4	149	1382

No.	Subduction Zone	Segment	Plate pairs	Left_E_LONG	Left_N_LAT	Left_REL_VEL (mm/yr)	Left_REL_AZI (°)	Right_E_LONG	Right_N_LAT	Right_REL_VEL (mm/yr)	Right_REL_AZI (°)	Length (km)
77	**Manokwari Trench**		PS\BH	132.515	0.017	21.8	206	129.197	1.059	15.0	210	389
78	**Halmahera**		MS\BH	126.426	1.706	100.9	116	125.969	-0.278	89.6	117	229
79	**Kepulauan Sangihe**		MS\SU	125.263	-0.446	16.5	288	126.426	1.706	5.0	264	282

Table 3.1 Continued.

No.	Subduction Zone	Segment	Dip (°)	Trench depth (km)	Updip_ pref (km)	Updip - min (km)	Updip – max (km)	Down-dip depth – pref (km)	Down-dip depth – min (km)	Down-dip depth – max (km)	Width – pref (km)	Width – min (km)	Width – max (km)	Coupling coefficient - pref
1	**Alaska/Aleutians**	**Whole Margin**	**14**	**6**	**12**	**6**	**24**	**40**	**26**	**48**	**122**	**30**	**192**	**0.55**
2	Alaska/Aleutians	Komandorski	15	5.5	10.5	5.5	24	35	25	45	95	30	153	0.5
3	Alaska/Aleutians	Western Aleutians	18	7	12	7	27	50	30	55	123	30	155	0.5
4	Alaska/Aleutians	Shumagin	14	6	11	6	16	26	20	32	62	30	107	0.2
5	Alaska/Aleutians	Semidi	14	6	11	6	24	30	25	50	79	30	182	0.7
6	Alaska/Aleutians	Kodiak	8	4.5	9.5	4.5	24.5	28	25	50	133	30	327	0.8
7	Alaska/Aleutians	Prince William Sound	6	4.5	14.5	4.5	24.5	42	25	50	263	30	435	0.8
8	Alaska/Aleutians	Yakataga	15	4	9	4	9	15	10	20	30	30	62	0.5
9	**Cascadia**		15	2.5	7.5	2.5	12.5	25	20	30	68	30	106	0.8
10	**Japan/Kurile**	**Whole Margin**	**16**	**8**	**12**	**8**	**14**	**50**	**40**	**61**	**142**	**97**	**197**	**0.77**
11	Japan/Kurile	Japan	15	7	7	7	7	50	40	65	166	128	224	0.7
12	Japan/Kurile	Kurile-Kamchatka	16	8	13	8	16	50	40	60	134	87	189	0.8
13	**Kanto**		15	1	6	1	9	25	20	30	73	43	112	0.9
14	**Nankai/Ryukyu**	**Whole Margin**	**15**	**5**	**10**	**5**	**13**	**22**	**17**	**27**	**45**	**31**	**83**	**0.44**
15	Nankai/Ryukyu	Nankai	15	3.5	8.5	3.5	11.5	25	20	30	64	33	102	0.9
16	Nankai/Ryukyu	Ryukyu	15	6	11	6	14	20	15	25	35	30	73	0.2
17	**Izu-Bonin**		15	7.5	12.5	7.5	15.5	35	25	45	87	37	145	0.2
18	**Marianas**		15	8	13	8	16	35	25	45	85	35	143	0.2
19	**North Yap**		15	7	12	7	15	35	25	45	89	39	147	0.2

No.	Subduction Zone	Segment	Dip (°)	Trench depth (km)	Updip_ pref (km)	Updip - min (km)	Updip – max (km)	Down-dip depth – pref (km)	Down-dip depth – min (km)	Down-dip depth – max (km)	Width – pref (km)	Width – min (km)	Width – max (km)	Coupling coefficient - pref
20	**Palau-South Yap**		15	5	10	5	13	35	25	45	97	46	155	0.2
21	**Hikurangi-Tonga-Kermadec**	**Whole margin**	**13**	**6**	**11**	**6**	**15**	**32**	**20**	**41**	**91**	**38**	**154**	**0.31**
22	H-K-T	Hikurangi	10	2.5	7.5	2.5	12.5	30	25	35	130	72	187	0.54
23	H-K-T	Kermadec	12	7	12	7	15	30	15	40	87	30	159	0.3
24	H-K-T	Tonga	17	8	13	8	16	35	25	45	75	31	127	0.2
25	**Puysegur**		15	5	10	5	13	35	30	45	97	66	155	0.7
26	**Hjort**		22	6	11	6	14	20	15	25	30	30	51	0.5
27	**Solomons**	**Whole margin**	**26**	**3.6**	**8.6**	**3.6**	**11.6**	**40**	**35**	**60**	**72**	**53**	**129**	**0.70**
28	Solomon	Northwest	26	6	11	6	14	40	35	60	66	48	123	0.7
29	Solomon	Southeast	26	2.5	7.5	2.5	10.5	40	35	60	74	56	131	0.7
30	**New Hebrides**	**Whole Margin**	**24**	**6.0**	**11**	**6**	**14**	**31**	**25**	**35**	**51**	**33**	**74**	**0.37**
31	New Hebrides	North	23	6	11	6	14	30	25	40	49	30	87	0.25
32	New Hebrides	Central	23	6	11	6	14	40	30	45	74	41	100	0.7
33	New Hebrides	South	23	6	11	6	14	30	25	40	49	30	87	0.25
34	New Hebrides	Matthew-Hunter	28	6	11	6	14	25	20	30	30	13	51	0.25
35	**New Britain**		26	6.5	11.5	6.5	14.5	40	30	50	65	35	99	0.7
36	**New Guinea Trench**	**Whole Margin**	**15**	**3.6**	**8.6**	**3.6**	**11.6**	**35**	**25**	**45**	**102**	**52**	**160**	**0.70**
37	NGT	East	15	3	8	3	11	35	25	45	104	54	162	0.7
38	NGT	West	15	4	9	4	12	35	25	45	100	50	158	0.7
39	**Manus Tr.**	**Whole Margin**	**15**	**3.5**	**8.5**	**3.5**	**11.5**	**35**	**25**	**45**	**102**	**52**	**160**	**0.50**
40	Manus Tr.	East	15	3.5	8.5	3.5	11.5	35	25	45	102	52	160	0.5

No.	Subduction Zone	Segment	Dip (°)	Trench depth (km)	Updip_ pref (km)	Updip - min (km)	Updip – max (km)	Down-dip depth – pref (km)	Down-dip depth – min (km)	Down-dip depth – max (km)	Width – pref (km)	Width – min (km)	Width – max (km)	Coupling coefficient - pref
41	Manus Tr.	West	15	3.5	8.5	3.5	11.5	35	25	45	102	52	160	0.5
42	**Andaman-Sunda Trench**	**Whole Margin**	**14**	**4.4**	**7.6**	**4.4**	**12.3**	**32**	**26**	**45**	**102**	**57**	**163**	**0.54**
43	An-Sunda Tr.	Andaman	14	3	5	3	11	40	35	45	145	99	174	0.7
44	An-Sunda Tr.	Sumatra	14	5	10	5	13	35	25	50	103	50	186	0.8
45	An-Sunda Tr.	Java	15	5	8	5	13	25	20	40	66	30	135	0.2
46	**Calabria**		20	4	10	4	12	45	40	60	102	82	164	0.5
47	**Hellenic Tr.**	**Whole Margin**	**35**	**24**	**17**	**2.4**	**10.4**	**45**	**40**	**50**	**50**	**53**	**86**	**0.60**
48	Hellenic	western segment	30	2	17	2	10	45	40	50	56	60	96	0.6
49	Hellenic	eastern segment	42	3	17	3	11	45	40	50	42	43	70	0.6
50	**Cyprus**	western segment	39	2	10	2	10	50	40	60	64	48	92	0.5
51	**Cyprus**	eastern segment	42	2	10	2	10	50	40	60	60	45	87	0.5
52	**Makran**		8	3	9	3	11	35	30	40	187	137	266	0.5
53	**S. America**	**Whole Margin**	**14**	**5**	**10**	**5**	**13**	**50**	**40**	**60**	**172**	**116**	**236**	**0.80**
54	S. America	Ecuador-Colombia	15	3	8	3	11	50	40	60	162	112	220	0.8
55	S. America	Peru	13	5	10	5	13	50	40	60	178	120	244	0.8
56	S. America	N. Chile	15	6	11	6	14	50	40	60	151	100	209	0.8
57	S. America	Central Chile	12	5	10	5	13	50	40	60	192	130	265	0.8
58	**Patagonia**	**Whole Margin**	**15**	**4**	**9**	**4**	**12**	**35**	**25**	**45**	**100**	**50**	**158**	**0.5**
59	Patagonia	North	15	4	9	4	12	35	25	45	100	50	158	0.5

No.	Subduction Zone	Segment	Dip (°)	Trench depth (km)	Updip_ pref (km)	Updip - min (km)	Updip – max (km)	Down-dip depth – pref (km)	Down-dip depth – min (km)	Down-dip depth – max (km)	Width – pref (km)	Width – min (km)	Width – max (km)	Coupling coefficient - pref
60	Patagonia	South	15	4	9	4	12	35	25	45	100	50	158	0.5
61	**South Shetland**		15	3	8	3	11	35	25	45	104	54	162	0.5
62	**South Sandwich**		15	7	12	7	15	35	25	45	89	39	147	0.2
63	**Mexico/Central America**	**Whole Margin**	**35**	**2.4**	**17**	**2.4**	**10.4**	**45**	**40**	**50**	**50**	**53**	**86**	**0.60**
64	Mexico/CA	Jalisco	16	4	9	4	12	25	20	35	58	30	112	0.5
65	Mexico/CA	Michoacan-Guatemala	16	4	9	4	12	20	15	30	40	30	94	0.7
66	Mexico/CA	El Salvador-Nicaragua	21	5	10	5	13	25	20	35	42	30	84	0.3
67	Mexico/CA	Costa Rica-west Panama	15	2.5	7.5	2.5	10.5	25	20	35	68	37	126	0.5
68	**Antilles**		15	4.5	9.5	4.5	12.5	35	25	45	99	48	156	0.5
69	**Manila**		15	4	9	4	12	35	25	45	100	50	158	0.15
70	**Philippine**		25	6	11	6	14	35	25	45	57	30	92	0.25
71	**East Luzon Trough**		20	5	10	5	13	35	25	45	73	35	117	0.5
72	**Cotabato Trench**		15	4	9	4	12	35	25	45	100	50	158	0.5
73	**Sulu Trench**		15	4	9	4	12	35	25	45	100	50	158	0.5
74	**Minahassa Trench**		15	3.5	8.5	3.5	11.5	35	25	45	102	52	160	0.5
75	**Seram Trough**		15	6	11	6	14	35	25	45	93	43	151	0.5
76	**Timor**		15	3	8	3	11	35	25	45	104	54	162	0.5

No.	Subduction Zone	Segment	Dip (°)	Trench depth (km)	Updip_ pref (km)	Updip - min (km)	Updip – max (km)	Down-dip depth – pref (km)	Down-dip depth – min (km)	Down-dip depth – max (km)	Width – pref (km)	Width – min (km)	Width – max (km)	Coupling coefficient - pref
77	**Manokwari Trench**		15	4	9	4	12	35	25	45	100	50	158	0.5
78	**Halmahera**		15	2	7	2	10	35	25	45	108	58	166	0.5
79	**Kepulauan Sangihe**		15	2	7	2	10	35	25	45	108	58	166	0.5

Table 3.1 Continued.

No	Subduction Zone	Segment	Coupling coefficient - min	Coupling coefficient - max	Mmax - pref	Mmax - min	Mmax - max	B-value - pref	B-value - min	B-value - max
1	**Alaska/Aleutians**	**Whole Margin**	**0.42**	**0.77**	**9.40**	**9.20**	**9.60**	**0.93**	**0.67**	**1.20**
2	Alaska/Aleutians	Komandorski	0.30	0.70	8.40	8.00	8.80	0.95	0.70	1.20
3	Alaska/Aleutians	Western Aleutians	0.30	0.70	9.40	9.20	9.60	0.92	0.63	1.20
4	Alaska/Aleutians	Shumagin	0.10	0.70	7.93	7.50	8.35	0.95	0.70	1.20
5	Alaska/Aleutians	Semidi	0.60	0.90	8.50	8.34	8.50	0.95	0.70	1.20
6	Alaska/Aleutians	Kodiak	0.90	1.00	9.20	8.63	9.20	0.95	0.70	1.20
7	Alaska/Aleutians	Prince William Sound	0.90	1.00	9.20	9.00	9.20	0.95	0.70	1.20
8	Alaska/Aleutians	Yakataga	0.30	0.70	8.10	8.00	8.10	0.95	0.70	1.20
9	**Cascadia**		0.70	0.90	9.00	8.80	9.20	0.95	0.70	1.20
10	**Japan/Kurile**	**Whole Margin**	**0.67**	**0.90**	**9.30**	**9.00**	**9.60**	**0.91**	**0.62**	**1.20**
11	Japan/Kurile	Japan Trench	0.60	0.90	9.08	9.00	9.16	0.91	0.61	1.20
12	Japan/Kurile	Kurile-Kamchatka	0.70	0.90	9.30	9.00	9.60	0.92	0.63	1.20
13	**Kanto**		0.80	1.00	8.21	8.00	8.42	0.95	0.70	1.20
14	**Nankai/Ryukyu**	**Whole Margin**	**0.34**	**0.80**	**8.95**	**8.50**	**9.41**	**0.91**	**0.61**	**1.20**
15	Nankai		0.80	1.00	8.70	8.50	8.90	0.91	0.61	1.20
16	Ryukyu		0.10	0.70	8.54	8.00	9.09	0.91	0.61	1.20
17	**Izu-Bonin**		0.10	0.70	8.21	7.20	9.21	0.95	0.70	1.20
18	**Marianas**		0.10	0.70	8.34	7.20	9.48	1.08	0.68	1.47
19	**North Yap**		0.10	0.70	8.07	7.20	8.93	0.95	0.70	1.20
20	**Palau-South Yap**		0.10	0.70	8.02	7.20	8.83	0.95	0.70	1.20
21	**Hikurangi-Kermadec-Tonga**	**Whole Margin**	**0.21**	**0.72**	**8.85**	**8.10**	**9.60**	**0.95**	**0.70**	**1.21**

No	Subduction Zone	Segment	Coupling coefficient - min	Coupling coefficient - max	Mmax - pref	Mmax - min	Mmax - max	B-value - pref	B-value - min	B-value - max
22	H-K-T	Hikurangi	0.40	0.70	8.50	8.00	9.00	0.95	0.70	1.20
23	H-K-T	Kermadec	0.20	0.75	8.76	8.10	9.42	0.96	0.70	1.21
24	H-K-T	Tonga	0.10	0.70	8.58	8.00	9.17	0.96	0.70	1.21
25	**Puysegur**		0.50	0.80	8.43	7.80	9.07	0.95	0.70	1.20
26	**Hjort**		0.30	0.70	7.78	7.20	8.36	0.95	0.70	1.20
27	**Solomon**	**Whole Margin**	**0.60**	**0.80**	**8.70**	**8.10**	**9.31**	**0.90**	**0.60**	**1.20**
28	Solomon	Northwest	0.60	0.80	8.36	8.10	8.62	0.90	0.60	1.20
29	Solomon	Southeast	0.60	0.80	8.60	8.10	9.09	0.90	0.60	1.20
30	**New Hebrides**	**Whole Margin**	**0.27**	**0.73**	**8.83**	**8.30**	**9.37**	**0.90**	**0.60**	**1.20**
31	New Hebrides	North	0.15	0.70	8.02	7.60	8.44	0.90	0.60	1.20
32	New Hebrides	Central	0.6	0.80	8.50	8.30	8.70	0.90	0.60	1.20
33	New Hebrides	South	0.15	0.70	8.12	7.60	8.64	0.90	0.60	1.20
34	New Hebrides	Matthew-Hunter	0.15	0.70	8.19	8.00	8.39	0.90	0.60	1.20
35	**New Britain**		0.60	0.80	8.41	8.00	8.82	0.90	0.60	1.20
36	**New Guinea Trench**	**Whole Margin**	**0.60**	**0.80**	**8.78**	**8.20**	**9.37**	**0.95**	**0.70**	**1.20**
37	New Guinea Trench	East	0.60	0.80	8.25	7.60	8.90	0.95	0.70	1.20
38	New Guinea Trench	west	0.60	0.80	8.61	8.20	9.03	0.95	0.70	1.20
39	**Manus**	**Whole Margin**	**0.30**	**0.70**	**8.50**	**7.50**	**9.50**	**0.95**	**0.70**	**1.20**
40	Manus	East	0.30	0.70	8.28	7.50	9.07	0.95	0.70	1.20
41	Manus	West	0.30	0.70	8.31	7.50	9.13	0.95	0.70	1.20
42	**Andaman-Sunda Trench**	**Whole Margin**	**0.44**	**0.79**	**9.30**	**9.00**	**9.60**	**0.94**	**0.67**	**1.20**
43	Andaman-Sunda	Andaman	0.60	0.80	9.30	9.00	9.55	0.94	0.67	1.20
44	Andaman-Sunda	Sumatra	0.70	0.90	9.20	9.00	9.40	0.94	0.67	1.20
45	Andaman-Sunda	Java	0.10	0.70	8.61	7.80	9.42	0.94	0.67	1.20

No	Subduction Zone	Segment	Coupling coefficient - min	Coupling coefficient - max	Mmax - pref	Mmax - min	Mmax - max	B-value - pref	B-value - min	B-value - max
46	**Calabria**		0.30	0.70	7.74	7.10	8.38	0.95	0.70	1.20
47	**Hellenic Trench**	**Whole margin**	**0.20**	**1.00**	**8.50**	**8.00**	**9.00**	**0.95**	0.69	**1.20**
48	Hellenic	western segment	0.20	1.00	8.37	8.00	8.74	0.95	0.69	1.20
49	Hellenic	eastern segment	0.20	1.00	8.21	8.00	8.42	0.95	0.69	1.20
50	**Cyprus**	western segment	0.30	0.70	8.00	7.50	8.49	0.95	0.70	1.20
51	**Cyprus**	eastern segment	0.30	0.70	7.89	7.50	8.29	0.95	0.70	1.20
52	**Makran**		0.30	0.70	8.71	8.10	9.33	0.95	0.69	1.20
53	**South America**	**Whole Margin**	**0.70**	**0.90**	**9.55**	**9.50**	**9.60**	**0.88**	**0.56**	**1.20**
54	S. America	Ecuador-Colombia	0.70	0.90	9.14	8.80	9.49	0.95	0.70	1.20
55	S. America	Peru	0.70	0.90	9.30	9.00	9.60	0.87	0.53	1.20
56	S. America	N. Chile	0.70	0.90	9.05	8.60	9.49	0.87	0.53	1.20
57	S. America	Central Chile	0.70	0.90	9.51	9.50	9.53	0.87	0.53	1.20
58	**Patagonia**	**Whole Margin**	**0.30**	**0.70**	**8.80**	**8.00**	**9.60**	**0.95**	**0.70**	**1.20**
59	Patagonia	North	0.30	0.70	8.50	8.00	9.00	0.95	0.70	1.20
60	Patagonia	South	0.30	0.70	8.72	8.00	9.45	0.95	0.70	1.20
61	**South Shetland**		0.30	0.70	8.11	7.50	8.71	0.95	0.70	1.20
62	**South Sandwich**		0.10	0.70	8.26	7.50	9.01	1.09	0.70	1.48
63	**Mexico/Central America**	**Whole Margin**	**0.37**	**0.81**	**8.90**	**8.20**	**9.60**	**0.91**	**0.62**	**1.20**
64	Mexico/CA	Jalisco	0.30	0.70	8.34	8.20	8.49	0.89	0.58	1.20
65	Mexico/CA	Michoacan-Guatemala	0.50	0.90	8.61	8.00	9.23	0.89	0.58	1.20
66	Mexico/CA	El Salvador-Nicaragua	0.10	0.70	8.29	8.00	8.58	0.95	0.70	1.20

No	Subduction Zone	Segment	Coupling coefficient - min	Coupling coefficient - max	Mmax - pref	Mmax - min	Mmax - max	B-value - pref	B-value - min	B-value - max
67	Mexico/CA	Costa Rica-west Panama	0.30	0.70	8.20	7.70	8.71	0.95	0.69	1.20
68	**Antilles**		0.30	0.70	8.69	8.00	9.37	0.92	0.64	1.20
69	**Manila**		0.05	0.70	8.25	7.60	8.90	0.95	0.70	1.20
70	**Philippine**		0.10	0.75	8.45	7.60	9.30	0.94	0.68	1.20
71	**East Luzon Trough**		0.30	0.70	7.84	7.30	8.38	0.95	0.70	1.20
72	**Cotabato Trench**		0.30	0.70	8.19	8.00	8.38	0.95	0.70	1.20
73	**Sulu Trench**		0.30	0.70	8.36	8.00	8.72	0.95	0.70	1.20
74	**Minahassa Trench**		0.30	0.70	8.39	7.90	8.89	0.95	0.70	1.20
75	**Seram Trough**		0.30	0.70	8.50	8.00	9.04	0.95	0.70	1.20
76	**Timor**		0.30	0.70	8.00	7.50	9.38	0.95	0.70	1.20
77	**Manokwari Trench**		0.30	0.70	8.12	7.60	8.64	0.95	0.70	1.20
78	**Halmahera**		0.30	0.70	8.33	8.30	8.35	0.95	0.70	1.20
79	**Kepulauan Sangihe**		0.30	0.70	8.39	8.30	8.47	0.95	0.70	1.20

Table 3.2 Compilation of published subduction interface zone b-values.

"Bayrak" values are from Bayrak et al. (2002), "Hayes" values were calculated by Gavin Hayes (USGS) as part of this GEM exercise, and the superscripts on the b-values in the "other" column refer to the following papers: [1]Power et al,(2012); [2]Cao and Gao (2002), [3]Suckale and Grünthal (2009); [4]Ghosh et al. (2008), [5]Bird and Kagan (2004) (which uses all shallow seismicity including plate-bending earthquakes); [6]Molchan et al. (1997) (note on Molchan et al. (1997); we use the b-values determined from mainshocks only, see their Table 1)

Subduction Zone	Bayrak	Hayes	other
Aleutian Trench	0.63	0.94	
Middle America Trench/Mexico	0.58	0.69	
Antilles Trench	0.64		
Peru-Chile Trench	0.53	0.71	
Tonga Trench	0.72	1.21	
Kermadec Trench		1.21	1.12[1]
South Sandwich Trench	0.74	1.48	
Hellenic Trench	0.69		
Makran Trench	0.78		
Sunda Trench (Sumatra-Java)	0.67	0.69	
Philippine Trench	0.68	0.84	
Nankai Trough/Ryukyu Trench	0.61	0.9	
Kurile Trench	0.63	0.81	
Japan Trench	0.61	0.81	0.73-0.86[2]
Mariana Trench	0.68	1.47	
New Hebrides	0.6	0.95	0.71[3]
Solomon Islands/New Britain	0.6	0.95	
Costa Rica		0.69	1.06[4]
Global Subduction Zones			0.96[5]
Global Subduction zones (<15 km)			0.93[6]
Global Subduction zones (16-33 km)			0.63[6]
Global Subduction zones (34-70 km)			0.83[6]

4 Discussion and Conclusions

Subduction zone earthquakes release approximately 90% of the long-term seismic moment outside of collision belts (Bird and Kagan, 2004). Here, we have reported on the development of a globally consistent characterisation of the world's subduction plate boundary interfaces. This can be used by seismic hazard analysts as a basis for generating earthquake event sets for inclusion in earthquake hazard and risk modelling.

In this report we assess the parameters associated with the plate interface itself and do not include seismicity within the down-going plate or overriding plate. To accurately estimate the total hazard associated with subduction zones, one also needs to consider plate-bending earthquakes and earthquakes associated with deformation of the down-going plate before it enters the subduction zone – so-called 'outer rise' events, as well as events occurring in the upper plate. These are outside of the scope of this report.

Using geophysical data, supplemented by the past history of earthquakes in subduction zones, a database has been developed to derive earthquake event sets on any segment of the globe's 55,000-km-long subduction interface zones. We have defined the likely maximum magnitude earthquake that could occur, the ratio of small to large earthquakes typical of each region (the Gutenberg-Richter b-value), a seismic coupling coefficient, and the relative plate velocity. Event sets for any subduction zone can then be created from these, consistently-derived, simple parameters.

The maximum magnitude of each subduction zone is based on its total length (McCaffrey, 2008). If the total length of the subduction zone exceeds what can realistically rupture with the generally accepted maximum magnitude around Mw 9.6 (e.g., Kagan and Jackson, 2013; Rong et al., 2014) then the Mmax is capped at this. When implemented, we propose that the earthquake event sets should 'float' along the whole subduction zone in the manner developed by Parsons et al. (2012) for the Nankai Trench in Japan, with the moment rate balanced against the convergence rates, coupling coefficients.

In this database we have defined suitably large uncertainties to encompass the plausible range of values to the input parameters and thus envelope the hazard posed by the subduction interface seismic zones. The database thus derived suggests that earthquakes above Mw 9 could be expected in as many 50% of the global subduction zones and their possible segments, consistent with the growing awareness that the historic period has been too short to accurately characterise the largest earthquakes on many of the subduction interface zones worldwide.

Acknowledgments

This report has benefited greatly from comments by Harold Magistrale and Yufang Rong of FM Global, and Annemarie Christophersen and Yoshihiro Kaneko of GNS Science.

References

Abercrombie, R. E., M. Antolik, K. Felzer, and G. Ekstrom (2001), The 1994 Java tsunami earthquake: Slip over a subducting seamount, J. Geophys. Res., 106, 6595–6607.

Ambraseys, N. N. and R. D. Adams (2001), The Seismicity of Central America, Imperial College Press, London, 309 pp.

Ammon, C. J., H. Kanamori, T. Lay, and A. A. Velasco (2006), The 17 July 2006 Java tsunami earthquake, Geophys. Res. Lett., 33, L24308, doi:10.1029/2006GL028005.

Ando, M., (1975), Source mechanisms and tectonic significance of historical earthquakes along the Nankai Trough, Japan, Tectonophys., v. 27(2), 119-140.

Ando, M., M. Nakamura, T. Matsumoto, M. furukawa, K. Tadokoro, and M. Furumoto (2009), Is the Ryukyu subduction zone in Japan coupled or decoupled? – The necessity of seafloor crustal deformation observation, Earth Planets and Space, 61, 1031-1039.

Basili R., Kastelic V., Demircioglu M. B., Garcia Moreno D., Nemser E. S., Petricca P., Sboras S. P., Besana-Ostman G. M., Cabral J., Camelbeeck T., Caputo R., Danciu L., Domac H., Fonseca J., García-Mayordomo J., Giardini D., Glavatovic B., Gulen L., Ince Y., Pavlides S., Sesetyan K., Tarabusi G., Tiberti M. M., Utkucu M., Valensise G., Vanneste K., Vilanova S., Wössner J. (2013a), The European Database of Seismogenic Faults (EDSF) compiled in the framework of the Project SHARE. http://diss.rm.ingv.it/share-edsf/, doi: 10.6092/INGV.IT-SHARE-EDSF.

Basili, R., M. M. Tiberti, V. Kastelic, F. Romano, A. Piatanesi, J. Selva, S. Lorito (2013b), Integrating geologic fault data into tsunami hazard studies. Nat. Hazards Earth Syst. Sci., 13(4), 1025-1050, doi: 10.5194/nhess-13-1025-2013.

Bayrak, Y., A. Yilmazturk, S. Ozturk (2002), Lateral variations of the modal (a/b) values for the different regions of the world, Journal of Geodynamics, 34, 653-666.

Beavan, J., S. Samsonov, P. Denys, R. Sutherland, N. Palmer, and M. Denham (2010a), Oblique slip on the Puysegur subduction interface in the 2009 July Mw 7.8 Dusky Sound earthquake from GPS and InSAR observations; implications for the tectonics of southwestern New Zealand, Geophys. J. Int., 183, 1265-1286.

Beavan, J., D. Silcock, M. Hamburger, E. G. Ramos, C. Thibault, and R. Feir, (2001), Geodetic constraints on postseismic deformation following the 1990 Ms 7.8 Luzon earthquake and implications for Luzon tectonics and Philippine Sea plate motion, Geochem. Geophys. Geosyst., vol. 2.

Beavan, J., X. Wang, C. Holden, K. Wilson, W. Power, G. Prasetya, M. Bevis, and R. Kautoke (2010b), Near-simultaneous great earthquakes at Tongan megathrust and outer rise in September 2009, Nature, 466, doi:10.1038/nature09292.

Bernard, P. and J. Lambert (1988), Subduction and seismic hazard in the northern Lesser Antilles: Revision of the historical seismicity, Bull. Seism. Soc. America, 78, 1965-1983.

Bilek, S. (2010), Seismicity along the South American subduction zone: Review of large earthquakes, tsunamis, and subduction zone complexity, Tectonphys, doi:10.1016/j.tecto.2009.02.037.

Bird, P. (2003), An updated digital model of plate boundaries, Geochem. Geophys. Geosystems 4, 1027, doi 10.1029/2001GC000252.

Bird, P., and Y.Y. Kagan (2004), Plate tectonic analysis of shallow seismicity: Apparent boundary width, beta, corner magnitude, coupled lithosphere thickness, and coupling in seven tectonic settings, Bull. Seis. Soc. America, 94(6), 2380-2399.

Bird, P., Y. Y. Kagan, D. D. Jackson, F. P. Schoenberg, and M. J. Werner (2009), Linear and nonlinear relations between relative plate velocity and seismicity, Bull. Seismol. Soc. Am., 99, 3097–3113, doi:10.1785/0120090082.

Byrne, D. E., L. R. Sykes, and D. M. Davies (1992), Great thrust earthquakes and aseismic slip along the plate boundary of the Makran subduction zone, J. Geophys. Res., 97(B1), 449–478, doi:10.1029/91JB02165.

Cagnan, Z., and G. Tanircan (2010), Seismic hazard assessment for Cyprus, J. Seismol., 14, 2, 225-246, 10.1007/s10950-009-9163-1.

Cao, A., and S.S. Gao, 2002, Temporal variation of seismic b-values beneath the northeastern Japan island Arc, Geophysical Research Letters, 29(9), 1334, doi: 10.1029/2001GL013775

Cifuentes, I. L., and P. G. Silver (1989), Low-frequency source characteristics of the great 1960 Chilean earthquake, J. Geophys. Res., 94(B1), 643–663, *doi:*10.1029/JB094iB01p00643.

Cornell, C. A. (1968), Engineering seismic risk analysis. Bull. Seismol. Soc. Am., 58, 1583–1606.

D'Agostino, N., and G. Selvaggi (2004), Crustal motion along the Eurasia-Nubia plate boundary in the Calabrian Arc and Sicily and active extension in the Messina Straits from GPS measurements, J. Geophys. Res., 109, B11402, 10.1029/2004JB002998.

D'Agostino, N., E. D'Anastasio, A. Gervasi, I. Guerra, M. R. Nedimovic, L. Seeber, and M. Steckler (2011), Forearc extension and slow rollback of the Calabrian Arc from GPS measurements, Geophys. Res. Lett., 38, 17, L17304, 10.1029/2011GL048270.

DeMets, C., R.G. Gordon, and D.F. Argus (2010), Geologically current plate motions, Geophys. J. Int., doi: 10.1111/j.1365-246X.2009.04491.x

Devoti, R., F. Riguzzi, M. Cuffaro and C. Doglioni (2008), New GPS constraints on the kinematics of the Apennines subduction. Earth Planet. Sc. Lett., 273, 163-174.

Fedotov, S. A., A. V. Solomatin, and S. D. Chernyshev (2007), Long-term earthquake prediction for the Kuril-Kamchatka arc for 2006–2011 and successful prediction for the Middle Kuril Island earthquake, 15.11.2006, Ms =8.2, J. Volcanol. Seismol., 1(3), 143–163, doi:10.1134/S0742046307030013.

Fournier, T. J., and J. T. Freymueller (2007), Transition from locked to creeping subduction in the Shumagin region, Alaska, Geophys. Res. Lett., 34, L06303, doi:10.1029/2006GL029073.

Frankel, A. and W. McCann (1979), Moderate and large earthquakes in the South Sandwich Arc: Indicators of tectonic variation along a subudction zone, J. Geophys. Res., 84 (B10), 5571-5577.

Frankel, A.D., and M.D. Petersen (2007), Cascadia Subduction Zone, U. S. Geol. Surv. Open File Rep. 2007-1437-L.

Fujii, Y., and K. Satake (2006), Source of the July 2006 West Java tsunami estimated from tide gauge records, Geophys. Res. Lett., 33, L24317, doi:10.1029/2006GL028049.

Galgana, G., M. Hamburger, R. McCaffrey, E. Corpuz, Q. Chen (2007), Analysis of crustal deformation in Luzon, Philippines using geodetic observations and earthquake focal mechanisms, Tectonophysics. 432, 63-87.

Ganas, A., and T. Parsons (2009), Three-dimensional model of Hellenic Arc deformation and origin of the Cretan uplift, J. Geophys. Res., 114, B06404, doi:10.1029/2008JB005599.

Ghosh, A., A. V. Newman, A. M. Thomas, and G. T. Farmer (2008), Interface locking along the subduction megathrust from b-value mapping near Nicoya Peninsula, Costa Rica, Geophys. Res. Lett., 35, L01301, doi:10.1029/2007GL031617.

Goldfinger, C., C.H. Nelson, A.E. Morey, J.R. Johnson, J. Patton, E Karabanov, J Gutierrez-Pastor, A.T. Eriksson, E Gracia, G. Dunhill, R.J., Enkin, A. Dallimore, and T. Vallier (2012), Turbidite event history—Methods and implications for Holocene paleoseismicity of the Cascadia subduction zone: U.S. Geological Survey Professional Paper 1661–F, 170 p, 64 figures, available at http://pubs.usgs.gov/pp/pp1661/f.

Guidoboni, E. and A. Comastri. (1997), The large earthquake of 8 August 1303 in Crete: seismic scenario and tsunami in the Mediterranean, J. Seismol., 1, 55–72.

Guidoboni, E., and A. Comastri (2005), Catalogue of earthquakes and tsunamis in the Mediterranean area from the 11th to the 15th century. Istituto Nazionale di Geofisica e Vulcanologia – SGA, Bologna, 1037 pp.

Guidoboni, E., G. Ferrari, D. Mariotti, A. Comastri, G. Tarabusi and G. Valensise (2007), CFTI4Med, Catalogue of Strong Earthquakes in Italy (461 B.C.-1997) and Mediterranean Area (760 B.C.-1500). INGV-SGA. Available from http://storing.ingv.it/cfti4med/.

Hamburger, M. W., R. K. Cardwell, and B. L. Isacks, Seismotectonics of the northern Philippine island arc, in The Tectonic and Geologic Evolution of Southeast Asian Seas and Islands: Part 2, Geophys. Monogr. Ser., vol. 27, edited by D. Hayes et al., pp. 1 – 22, AGU, Washington, D. C., 1983.

Hanks, T. C., G. C. Beroza, and S. Toda (2012), Have recent earthquakes exposed flaws in or misunderstandings of probabilistic seismic hazard analysis? Seismol. Res. Lett., 83, 759-764.

Hanks, T.C., and H. Kanamori (1979) A moment magnitude scale, Journal of Geophysical Research, Vol. 84B5, 2348-2350.

Hashimoto, C., A. Noda, T. Sagiya, and M. Matsu'ura (2009), Interplate seismogenic zones along the Kuril–Japan trench inferred from GPS data inversion, Nature Geoscience, 2, 141-144.

Hayes, G. P., D. J. Wald, and R. L. Johnson (2012), Slab1.0: A three-dimensional model of global subduction zone geometries, J. Geophys. Res., 117, B01302, doi:10.1029/2011JB008524.

Heidarzadeh, M., Pirooz, M.D., Zaker, N.H., Yalciner, A.C., Mokhtari, M., Esmaeily, A. (2008), Historical tsunami in the Makran Subduction Zone off the southern coasts of Iran and Pakistan and results of numerical modelling, Ocean Engineering, 35 (774-786).

Heuret, A. (2005), Dynamique des zones de subduction: Etude statistique globale et approche analogique—Subduction zones dynamics: Global statistical study and experimental modelling, Ph.D. thesis, Univ. Montpellier II, Montpellier, France. (Available at http://tel.archives-ouvertes.fr/tel-00108728/en/)

Heuret, A., S. Lallemand, F. Funiciello, C. Piromallo, and C. Faccenna (2011), Physical characteristics of subduction interface type seismogenic zones revisited. Geochemistry, Geophysics, Geosystems 12: Q01004, doi:10.1029/2010GC003230.

Hiemer, S., D.D. Jackson, Q. Wang, Y.Y. Kagan, J. Woessner, J.D. Zechar and S. Wiemer (2013), A stochastic forecast of California earthquakes based on fault slip and smoother seismicity. BSSA 103: 799-810.

Hollenstein, Ch., M.D. Müller, A. Geiger and H.-G. Kahle (2008), Crustal motion and deformation in Greece from a decade of GPS measurements, 1993–2003, Tectonophy., 449, 17–40, 10.1016/j.tecto.2007.12.006.

Ishii, M., P. M. Shearer, H. Houston, and J. E. Vidale (2005), Extent, duration and speed of the 2004 Sumatra-Andaman earthquake imaged by Hi-Net array, Nature, 435, 933–936, doi:10.1038/nature03675.

Ito, T., and M. Hashimoto (2004), Spatiotemporal distribution of interplate coupling in southwest Japan from inversion of geodetic data, J. Geophys. Res., 109, B02315, doi:10.1029/2002JB002358.

Johnson, J. M., Y. Tanioka, L. J. Ruff, K. Satake, H. Kanamori, and L. R. Sykes (1994), The great Aleutian earthquake, Pure Appl. Geophys., 142, 3–28, doi:10.1007/BF00875966.

Kagan, Y.Y., and D.D. Jackson (2013) Tohoku Earthquake: A Surprise?. BSSA 103: 1181 -1194.

Kanamori, H. (1986), Rupture process of subduction-zone earthquakes, Annu. Rev. Earth Planet. Sci., 14, 293–322, doi:10.1146/annurev.ea.14.050186.001453.

Koppa, C., J. Fruehn., E.R. Flueh., C. Reichert., N. Kukowski., J. Bialas., D. Klaeschen (2000), Structure of the Makran subduction zone from wide-angle and reflection seismic data, Tectonophys. 329, 171–191.

LaFemina, P., T. H. Dixon, R. Govers, E. Norabuena, H. Turner, A. Saballos, G. Mattioli, M. Protti, and W. Strauch (2009), Fore-arc motion and Cocos Ridge collision in Central America, Geochem. Geophys. Geosyst., 10, Q05S14, doi:10.1029/2008GC002181.

Larson, K., A.R. Lowry, V. Kostoglodov, W. Hutton, O. Sanchez, K. Hudnut, and G. Suarez (2004), Crustal deformation measurements in Guerrero, Mexico, J. Geophys. Res., 109(B04409).

Lay, T., and H. Kanamori (1980), Earthquake doublets in the Solomon Islands, Phys. Earth Planet. Int., 21, 283-304.

Lay, T., C.J. Ammon, H. Kanamori, L. Rivera, K.D. Koper, and A.R. Hutko, (2010), The 2009 Samoa-Tonga great earthquake triggered doublet, Nature, 466, 964-968.

Madariaga, R., M. Metois, C. Vigny, and J. Campos (2010), Central Chile finally breaks, Science, 328(5975), 181–182, doi:10.1126/science.1189197.0.

McCaffrey, R. (1997), Influences of recurrence times and fault zone temperature on the age-rate dependence of subduction zone seismicity, J. Geophys. Res., 102, 22,839–22,854, doi:10.1029/97JB01827.

McCaffrey, R., (2008), Global frequency of magnitude 9 earthquakes: Geol., v. 36, no. 3, p. 263-266.

McCaffrey, R., (2009), The tectonic framework of the Sumatran Subduction Zone, Annual Rev. Earth Planet. Sci., 37, 346-366.

McCann, W. R., S. P. Nishenko, L. R. Sykes, and J. Krause (1979), Seismic gaps and plate tectonics: Seismic potential for major boundaries, Pure Appl. Geophys., 117, 1082–1147, doi:10.1007/BF00876211.

Meckel, T. A., M. F. Coffin, S. Mosher, P. Symonds, G. Bernardel, and P. Mann (2003), Underthrusting at the Hjort Trench, Australian-Pacific plate boundary: Incipient subduction?, Geochem. Geophys. Geosyst., 4(12), 1099, doi:10.1029/2002GC000498.

Meckel, T. A., P. Mann, S. Mosher, and M. F. Coffin (2005), Influence of cumulative convergence on lithospheric thrust fault development and topography along the Australian-Pacific plate boundary south of New Zealand, Geochem. Geophys. Geosyst., 6, Q09010, doi:10.1029/2005GC000914.

Molchan, G., T. Kronrod, and G.F. Panza (1997), Multi-scale seismicity model for seismic risk, Bull. Seismol. Soc. of America, 87(5), 1220-1229.

Nishimura, T., T. Hirasawa, S. Miyazaki et al. (2004a), Temporal change of interplate coupling in northeastern japan during 1995−2002 estimated from continuous GPS observations, Geophys. J. Int., 157, 901−916.

Nishimura, S., M. Hashimoto, and M. Ando (2004b), A rigid block rotation model for the GPS derived velocity field along the Ryukyu arc, Phys. Earth Planet. Inter., 142, 185–203, doi:10.1016/j.pepi.2003.12.014.

Nishimura, T., T. Sagiya, and R. S. Stein (2007), Crustal block kinematics and seismic potential of the northernmost Philippine Sea plate and Izu microplate, central Japan, inferred from GPS and leveling data, J. Geophys. Res., 112, B05414, doi:10.1029/2005JB004102.

Norabuena, E., et al. (2004), Geodetic and seismic constraints on some seismogenic zone processes in Costa Rica, J. Geophys. Res., 109, B11403, doi:10.1029/2003JB002931.

Okal, E.A., and D. Reymond (2003), The mechanism of the great Banda Sea earthquake of 01 February 1938: Applying the method of Preliminary Determination of Focal Mechanism to a historical event, Earth Planet. Sci. Letts., 216, 1-15.

Pacheco, J. F., and S. K. Singh (2010), Seismicity and state of stress in Guerrero segment of the Mexican subduction zone, J. Geophys. Res., 115, B01303, doi:10.1029/2009JB006453.

Parsons, T., Console, R., Falcone, G., Murru, M., and Yamashita, K. (2012), Comparison of characteristic and Gutenberg-Richter models for time-dependent M ≥ 7.9 earthquake probability in the Nankai-Tokai subduction zone, Japan, Geophys. J. Int. 190, 1673-1688, doi: 10.1111/j.1365-246X.2012.05595.x

Park, S.-C., and J. Mori (2007), Are asperity patterns persistent? Implication from large earthquakes in Papua New Guinea, J. Geophys. Res., 112, B03303, doi:10.1029/2006JB004481.

Peterson, E. T., and T. Seno (1984), Factors affecting seismic moment release rates in subduction zones, J. Geophys. Res., 89, 10,233–10,248, doi:10.1029/JB089iB12p10233.

Power, W.L., L.M. Wallace., X. Wang., M.E. Reyners (2011), Tsunami hazard posed to New Zealand by the Kermadec and southern New Hebrides subduction margins : an assessment based on plate boundary kinematics, interseismic coupling, and historical seismicity. Pure and applied geophysics, doi:10.1007/s00024-011-0299-x.

Prawirodirdjo, L., R. McCaffrey, C. D. Chadwell, Y. Bock, and C. Subarya (2010), Geodetic observations of an earthquake cycle at the Sumatra subduction zone: Role of interseismic strain segmentation, J. Geophys. Res., 115, B03414, doi:10.1029/2008JB006139.

Reilinger, R., et al. (2006), GPS constraints on continental deformation in the Africa-Arabia-Eurasia continental collision zone and implications for the dynamics of plate interactions, J. Geophys. Res., 111, B05411, doi:10.1029/2005JB004051.

Rong Y, Jackson DD, Magistrale H, Goldfinger C (2014) Magnitude limits of subduction zone earthquakes. Bull. Seismol. Soc. Am. 104(5):2359-2377. doi:10.1785/0120130287.

Ruff, L. J. (1989), Do trench sediments affect great earthquake occurrence in subduction zones?, in Subduction Zones Part I, edited by L. J. Ruff and H. Kanamori, Pure Appl. Geophys., 129, 263–282.

Ruff, L. J., and H. Kanamori (1980), Seismicity and the subduction process, Phys. Earth Planet. Inter., 23, 240–252, doi:10.1016/0031-9201(80)90117-X.

Ruppert, N. A., J. M. Lees, N. P. Kozyreva (2007), Seismicity, earthquakes and structure along the Alaska-Aleutian and Kamchatka-Kutile subduction zones: A review, in Volcanism and Subduction: The Kamchatka Region, Geophys. Monogr. Ser., vol. 172, edited by J. Eichelberger et al., pp. 129–144, doi:10.1029/172GM12,AGU,Washington,D.C.

Sagiya, T., and W. Thatcher (1999), Coseismic slip resolution along a plate boundary megathrust: The Nankai Trough, southwest Japan, J. Geophys. Res., 104(B1), 1111-1129.

Scherwath, M., H. Kopp., E.R. Flueh., S.A Henrys., and R. Sutherland (2008), Structure and Deformation of the Hikurangi-Kermadec Subduction Zone - Transitions Revealed by Seismic Wide-angle Data. Eos Trans. AGU, 2008 Fall Meeting. Suppl., Abstract T23A-1997.

Schluter, H.U., A. Prexl., Ch. Gaedicke., H. Roeser., Ch. Reichert., H. Meyer., C. von Daniels (2002). The Makran accretionary wedge: sediment thicknesses and ages and the origin of mud volcanoes. Mar. Geol. 185, 219–232.

Scholz, C. H., and J. Campos (1995), On the mechanism of seismic decoupling and back-arc spreading at subduction zones, J. Geophys. Res., 100, 22,103–22,115, doi:10.1029/95JB01869.

Scholz, C. H., and J. Campos (2012), The seismic coupling of subduction zones revisited, J. Geophys. Res. 117, doi:10.1029/2011JB009003.

Schwartz, S. Y., T. Lay, and L. J. Ruff (1989), Source process of the great 1971 Solomon Islands doublet, Phys. Earth Planet. Inter., 56(3–4), 294–310, doi:10.1016/0031-9201 (89)90164-7.

Selvans, M., J. Stock, C. DeMets, O. Sanchez and B. Marquez-Azua, (2010), Constraints on Jalisco Block motion and tectonics of the Guadalajara Triple Junction from 1998-2001 campaign GPS data, PAGEOPH, DOI . 10.1007/s00024-010-0201-2, 201

Serpelloni, E., R. Burgmann, M. Anzidei, P. Baldi, B. Mastrolembo Ventura, and E. Boschi (2010), Strain accumulation across the Messina Straits and kinematics of Sicily and Calabria from GPS data and dislocation modeling. Earth Planet. Sc. Lett., 298, 3-4, 347-360, 10.1016/j.epsl.2010.08.005.

Shaw, B. and Jackson, J. (2010), Earthquake mechanisms and active tectonics of the Hellenic subduction zone. Geophys. J. Int., 181: 966–984. doi: 10.1111/j.1365-246X.2010.04551.x

Socquet, A., W. Simons, C. Vigny, R. McCaffrey, C. Subarya, D. Sarsito, B. Ambrosius, and W. Spakman (2006), Microblock rotations and fault coupling in SE Asia triple junction (Sulawesi, Indonesia) from GPS and earthquake slip vector data, J. Geophys. Res., 111, B08409, doi:10.1029/2005JB003963.

Stein, S., and E. A. Okal (2007), Ultralong period seismic study of the December 2004 Indian Ocean earthquake and implications for regional tectonics and the subduction process, Bull. Seismol. Soc. Am., 97(1A), S279–S295, doi:10.1785/0120050617.

Stein, S., R. J. Geller, and M. Liu (2012), Why earthquake hazard maps often fail and what to do about it. Tectonophysics, 562-563, 1-25.

Stirling, M.W., McVerry, G.H., Gerstenberger, M., Litchfield, N.J., Van Dissen, R., Berryman, K.R., Langridge, R.M., Nicol, A., Smith, W.D., Villamor, P., Wallace, L., Clark, K., Reyners, M., Barnes, P., Lamarche, G., Nodder, S., Pettinga, J., Bradley, B., Rhoades, D., Jacobs, K (2012), National Seismic Hazard Model for New Zealand: 2010 Update. Bull. Seismol. Soc. Am. 102(4), 1514-1542.

Subarya, C., M. Chlieh, L. Prawirodirdjo, J.-P. Avouac, Y. Bock, K. Sieh, A. J. Meltzner, D. H. Natawidjaja, and R. McCaffrey (2006), Plate boundary deformation associated with the great Sumatra-Andaman earthquake, Nature, 440(7080), 46–51, doi:10.1038/nature04522.

Suckale, J. and G. Grünthal (2009), A probabilistic seismic hazard model for Vanuatu, Bull. Seis. Soc. Am., 99, 4, 2108-2126.

Taylor, F.W., R.W. Briggs, C. Frohlich, A. Brown, M. Hornbach, A.K. Papabatu, A.J. Meltzner, and D. Billy, (2008a), Rupture across arc segment and plate boundaries in the 1 April 2007 Solomons earthquake, Nature Geoscience, 1, 253-257

Taylor, F. W., M. G. Bevis, I. W. D. Dalziel, R. Smalley Jr., C. Frohlich, E. Kendrick, J. Foster, D. Phillips, and K. Gudipati (2008b), Kinematics and segmentation of the South Shetland Islands-Bransfield basin system, northern Antarctic Peninsula, Geochem. Geophys. Geosyst., 9, Q04035, doi:10.1029/2007GC001873.

Tichelaar, B. W., and L. J. Ruff (1993), Depth of seismic coupling along subduction zones, J. Geophys. Res., 98, 2017–2037, doi:10.1029/92JB02045.

Tregoning, P., and A. Gorbatov (2004), Evidence for active subduction at the New Guinea Trench, Geophys. Res. Lett., 31, L13608, doi:10.1029/2004GL020190.

Utsu, T., Table of destructive earthquakes in the world, http://iisee. kenken.go.jp/utsu/, 1989.

Uyeda, S. and H. Kanamori (1979), Back-arc opening and the mode of subduction, J. Geophys. Res. 84, 1049-1061.

Vernant, P., and 11 co-authors, (2004), Present-day crustal deformation and plate kinematics in the Middle East constrained by GPS measurements in Iran and northern Oman, Geophys. J. Int., 157, 381-398.

Vigny, C., and 16 co-authors (2002), Migration of seismicity and earthquake interactions monitored by GPS in SE Asia triple junction: Sulawesi, Indonesia, J. Geophys. Res., 107(B10), 2231, doi:10.1029/2001JB000377.

Wald, D. J., and P. G. Somerville (1995), Variable-slip rupture model of the great 1923 Kanto, Japan earthquake: Geodetic and body-waveform analysis, Bull. Seismol. Soc. Am., 85, 159–177.

Wallace, L. M., J. Beavan., R. McCaffrey., and D. Darby (2004a), Subduction zone coupling and tectonic block rotations in the North Island, New Zealand: J. Geophys. Res., v. 109, no. B12406, p. doi:10.1029/2004JB003241.

Wallace, L. M., C. Stevens, E. Silver, R. McCaffrey, W. Loratung, S. Hasiata, R. Stanaway, R. Curley, R. Rosa, and J. Taugaloidi (2004b), GPS and seismological constraints on active tectonics and arc-continent collision in Papua New Guinea: Implications for mechanics of microplate rotations in a plate boundary zone, J. Geophys. Res., 109, B05404, doi:10.1029/2003JB002481.

Wallace, L.M., R. McCaffrey., J. Beavan., and S. Ellis (2005), Rapid microplate rotations and back-arc rifting at the transition between collision and subduction, Geology, 33(11), 857-860.

Wallace, L.M., R. J. Beavan., R. McCaffrey., K.R. Berryman., and P. Denys (2007), Balancing the plate motion budget in the South Island, New Zealand using GPS, geological and seismological data. Geophys. J. int., 168(1): doi:10.1111/j.1365-246X.2006.03183.x

Wallace, L. M., S. Ellis., K. Miyao., S. Miura., J. Beavan., and J. Goto (2009a), Enigmatic, highly active left-lateral shear zone in southwest Japan explained by aseismic ridge collision, Geol., 37(2), 143–146, doi:10.1130/G25221A.1.

Wallace, L. M., and 21 co-authors (2009b), Characterizing the seismogenic zone of a major plate boundary subduction thrust: Hikurangi Margin, New Zealand, Geochem. Geophys. Geosyst., 10.

Wdowinski, S., Z. Ben-Avraham, R. Arvidsson and G. Ekström (2006) Seismotectonics of the Cyprian Arc. Geophys. J. Int., 164, 1, 176-181, 10.1111/j.1365-246X.2005.02737.x

Wesson, R.L., O. S. Boyd., C. S. Mueller., C. G. Bufe., A. D. Frankel., and M. D. Petersen (2007), Revision of Time-Independent Probabilistic Seismic Hazard Maps for Alaska, USGS Open File Report 2007-1043.

Yolsal, S., T. Taymaz and A. C. YalÃ§iner (2007), Understanding tsunamis, potential source regions and tsunami-prone mechanisms in the Eastern Mediterranean. Geol. Soc. Spec. Publ., 291, 1, 201, 10.1144/SP291.10.

APPENDIX A Definition of Database Parameters

Subduction Zone: Name of subduction zone

Segment: Name of segment of the subduction zone. Note that these segments are not necessarily intended to represent rupture segments. They are largely chosen where a change in plate motion rate and azimuth undergoes a change, due to a change in the plate pairs that are juxtaposed at the boundary. The main exception to this is Alaska, where we define segments similar to the most recent USGS seismic hazard model for Alaska (Wesson et al., 2007).

Plate pairs: These are the plate pairs used in the calculation of convergence rate and azimuth on the subduction zone. In all cases, except where specified with an asterisk (*) in Table 3.1 the plate abbreviations conform to the tectonic model of Bird (2003), referred to as PB2002 for the remainder of these notes. Where there are exceptions, we detail those within the supplementary notes.

Left_E_LONG, Right_E_LONG: The longitude of the left- and right-hand sides (respectively) of the trench for the segment in this row. NOTE: The left and right hand endpoints of the trench are defined with an arbitrary convention such that when the subduction zone is rotated so that the trench is at the bottom, the volcanic arc is at the top, and the subducting plate moves relatively upward on the map.

Left_N_LAT, Right_N_Lat: The Latitude of the left- and right-hand sides (respectively) of the trench for this segment.

Left_REL_VEL, Right_REL_VEL: Horizontal relative plate velocity in mm/yr, on the left- and right-hand sides (respectively) of the trench, using the Plate pairs described in the Plate pairs column of Table 3.1. Unless otherwise noted (in the following notes) these relative plate velocities are derived from PB2002. If a source other than PB2002 is used, we detail the source in these notes.

Left_REL_AZI, Right_REL_AZI: Azimuth of relative plate convergence (on the left- and right-hand sides, respectively) assuming a fixed overriding plate. Azimuths are listed in degrees clockwise from local north. Unless otherwise noted in Appendix B these relative convergence azimuths are derived from PB2002. If a source other than PB2002 is used, we detail the source in these notes.

Length: Distance along trench between segment endpoints (in km).

Dip: Average dip angle for the seismogenic portion of the segment. Unless otherwise noted (see additional notes in Appendix B), the dips are determined from Hayes et al. (2012) database of global subduction zone geometries. Where we have no information about the dip angle, we use a default value of 15°.

Trench depth: Vertical distance (in km) of the trench from mean sea level.

Up-dip depth (Pref, Min, Max): Vertical distance (in km below sea level) to the up-dip limit of seismic rupture on the subduction interface (with preferred, minimum, and maximum values). In all cases, we use the intersection of the trench with the Earth's surface as a default "Up-dip depth-min" estimate, to account for the possibility that rupture to the trench cannot be ruled-out anywhere. We use 5 km below the intersection of the subduction interface and the seafloor as a default preferred value, and 8 km as a default maximum value where no other information is available. Where we use values that depart from these assumptions, we explain our choices in these notes. Where possible we use depths below sea level derived from Hayes et al. (2012) database of global subduction zone geometries.

Down-dip depth (Pref, Min, Max): Vertical distance (in km below sea level) to the down-dip limit of seismic rupture on the subduction interface (with preferred, minimum, and maximum values). For subduction zones where we do not have knowledge of this, we assume a default value of 35 ± 10 km. Where we use a value that departs from this assumption, we justify this in these notes. Where possible we use depths below sea level derived from Hayes et al. (2012) database of global subduction zone geometries.

Down-dip width (Pref, Min, Max): is the width along the dip of the interface (in km) of the seismogenic portion of the subduction interface. This is calculated using the interface dip, up-dip depths, and down-dip depths in previous columns.

Coupling Coefficient (Pref, Min, Max): is the seismic coupling coefficient (preferred, minimum, and maximum values) for the subduction interface segment. Coupling coefficient is the proportion of relative plate motion that will be eventually accommodated as seismic slip. Ideally, this is best determined from the knowledge of historic and prehistoric subduction interface ruptures, but the short records for most subduction zones do not allow a meaningful determination in this fashion. Therefore, where the megathrust locking ratio (the ratio of slip deficit rate to plate convergence rate) is available from interpretation of geodetic measurements (see Appendix B for delineation of which margins geodetic coupling estimates are available for), we use this value as a proxy for the seismic coupling coefficient. We are mindful of the fact that the physical meaning of the locking ratio and its relationship with the long-term seismic coupling coefficient is still uncertain, but we are not aware of other, better ways of defining the coupling coefficient at present. For each subduction zone we outline the sources of data used for the choice of coupling coefficients. At many subduction zones, it is not possible to determine coupling coefficients, either due to a lack of geodetic data, and/or a lack of sufficient historical seismicity data. We assign reasonably large uncertainties to those coupling coefficients. For subduction zones where the coupling coefficient is highly uncertain, we use a default value of 0.5 ± 0.2. We also do not allow the maximum coupling coefficient for any subduction zone to be less than 0.7, even when independent data (geodetic, historical seismicity) exists to help constrain this. This is to help incorporate our current lack of understanding of the relevance of contemporary estimates of coupling (from geodetic and historic seismicity studies) to the long-term subduction plate interface earthquake behaviour.

Mmax (Pref, Min, Max): the Maximum Magnitude earthquake expected for the subduction segment. For all segments, we assume a default maximum Mmax based on rupture length of the entire segment (or combination of segments), using the relationship between segment length and magnitude in McCaffrey (2008). The minimum Mmax value is taken as the largest earthquake observed in the historical record on that segment. For the preferred value, we take the average of the minimum and maximum Mmax values. For subduction zones where little or no seismicity or paleoseismological data exist to constrain Mmax, we generally assume 7.5 as a minimum Mmax. For all magnitudes discussed here, we use the moment magnitude scale of Hanks and Kanamori (1979).

b-value (Pref, Min, Max): Our understanding of b-values at subduction megathrusts is incomplete, and estimates from individual subduction zones range from ~0.6 to >1.2 (see Table 3.1). To encompass this uncertainty, we assume a minimum b-value for all subduction zones of 0.7, and a maximum of 1.2. In cases where published studies have estimated b-values that are less than 0.7, or exceed 1.2, we use the published values to inform the minimum or maximum value in our table.

APPENDIX B Additional notes on parameter choices for specific subduction zones/segments

*Note that the subduction zones/segments are not necessarily ordered in an identical manner as Table 3.1.

B.1 Alaska/Aleutian

Most of the parameter values we use in the spreadsheet are derived from Wesson et al. (2007). However, the coupling coefficients, dips, and down-dip limits for the Shumagin, Semidi, and Kodiak segments are derived directly from geodetic studies of Fournier and Freymueller (2007; their fault planes 3 and 4 combine to form the Shumagin segment, while plane 2 is the Semidi segment and plane 1 is the western part of the Kodiak segment). For the maximum down-dip limit we assume the maximum value in Wesson et al. (2007), and for the Kodiak and Semidi segments we assume a sigma on the coupling coefficient of 0.1. For the Prince William Sound segment, we base the minimum and maximum seismogenic depths (and their uncertainties) on the Mw 9.2 1964 Prince William Sound earthquake. Due to this segment's propensity to produce megathrust earthquakes Mw > 9.0, we assign a high coupling coefficient for this segment as well. Note that the segments are largely defined for kinematic and plate boundary geometry purposes; multiple segment rupture is possible and will be considered in any model.

The Wesson et al. (2007) report precedes the recent subduction margin studies which entertain the possibility of larger earthquakes than has been observed historically (e.g., McCaffrey, 2008). Therefore, in this report, we suggest it is prudent to allow for the possibility of larger ruptures than have occurred historically, which largely forms the basis of the Wesson et al. (2007) study. We indicate this in Table 3.1 as 'whole margin' rupture, but in fact the total length of the margin is longer than reasonably associated with the upper bound Mmax of 9.6. Therefore, we recommend that hazard analysts consider a logic tree approach and provide some weight to a model where earthquakes up to Mw 9.6 could occur anywhere along the Alaska-Aleutian subduction zone, and event sets respect the available seismic moment noting variation in coupling coefficient, convergence rates and small variation in b-value along the length of the subduction zone.

B.2 Cascadia

For down-dip depth and Mmax, we use values consistent with Frankel and Petersen (2007), and references therein. Based on geodetic evidence for high interseismic coupling coefficients on the megathrust (relevant studies discussed in Frankel and Petersen, 2007), we assign a high coupling coefficient (0.8 ± 0.1).

B.3 Japan

The coupling coefficients and seismogenic depths are based on interseismic modelling of geodetic data (Nishimura et al., 2004a; Hashimoto et al., 2009), and the updip limit and minimum Mmax values are based on the recent Mw 9.0 Tohoku earthquake.

B.4 Kanto

The coupling coefficients and down-dip limit of the seismogenic zone are based on interseismic modelling of geodetic data (Nishimura et al., 2007), and the maximum rupture depth of the 1923 M 7.9 Kanto earthquake (e.g., Wald and Somerville, 1995). The minimum Mmax value is based on the estimated M 8.0 Genroku earthquake in 1703.

B.5 Nankai

The down-dip limit of the Nankai Trough seismogenic zone is based on models of rupture in previous great earthquakes there (Ando, 1975; Sagiya and Thatcher, 1999) and models of interseismic coupling (Ito and Hashimoto, 2004). High coupling coefficients are justified on the basis of the interseismic coupling models from GPS and the large amount of plate boundary slip required in historic great earthquakes at the Nankai Trough. The minimum Mmax (8.5) is based on the largest historic events observed at the Nankai Trough, which involved simultaneous rupture of all segments of the Nankai Trough in a single event (Ando, 1975).

B.6 Kurile

Due to the propensity of this subduction zone to produce Mw 8.0 -9.0 earthquakes, we assign a high coupling coefficient. A minimum Mmax of 9.0 is used based on the largest historical earthquake on this subduction zone (the 1952 earthquake). However, due to the great length of this subduction zone, it certainly may be capable of generating larger events.

B.7 Ryukyu

Despite the very high convergence rates at the Ryukyu Trench (up to 130 mm/yr) no large historical earthquakes have occurred here (e.g., larger than Mw 8.0). Thus, we assign a relatively low coupling coefficient to the Ryukyu Trench. GPS measurements from Kyushu and the Ryukyu arc also suggest little or no interseismic coupling on the Ryukyu Trench (Nishimura et al., 2004b; Wallace et al., 2009a), although this is particularly difficult to resolve for most of the Ryukyu Trench due to the distance of land-based geodetic studies from portions of the thrust that could undergo interseismic locking (Ando et al., 2009). The largest historic earthquake thought to be on interface occurred in 1911 and is estimated to be M 8.0 (Utsu, 1989). The upper plate is rifted continental margin crust so we also include a relatively shallow down-dip limit to the seismogenic zone.

B.8 Izu-Bonin

No historic earthquakes larger than Mw 7.2 have been observed on the Izu-Bonin Trench. Due to the lack of significant historical subduction thrust events (and a prevalence of more frequent moderate magnitude events), we assign a low coupling coefficient (0.2 ± 0.1).

B.9 Mariana

No historic underthrusting earthquakes larger than Mw ~7.2 have been observed along the Mariana Trench. Due to the lack of significant historical subduction thrust events (and a prevalence of more frequent moderate magnitude events), we assign a low coupling coefficient (0.2 ± 0.1).

B.10 North Yap, and Palau/South Yap

Little is known about the seismogenic potential of these trenches. We assign similar values as for the Izu-Bonin-Marianas Trench. Convergence rates used are from DeMets et al. (2010), which has a more up to date Philippine Sea Plate model.

B.11 Hikurangi

The parameters for the Hikurangi subduction zone are largely derived from Wallace et al. (2004a; 2009b) and from the inputs for the Hikurangi subduction source to the updated New Zealand national seismic hazard model (Stirling et al., 2012). Although we treat the Hikurangi Trough as a single source in this spreadsheet, in the New Zealand seismic hazard model, it is treated as 3 segments, where the southern Hikurangi segment has a higher coupling coefficient than the central and northern segments. For the purposes of this study, we average the coupling coefficients over the length of the margin. The Mmax preferred is based on a plausible scenario where rupture of the entire southern Hikurangi segment occurs, which is currently interseismically coupled over a large area. The maximum Mmax is based on a scenario where rupture of the entire Hikurangi margin occurs in a single event, which would produce an Mw ~9.0 (Wallace et al., 2009b; Stirling et al., 2012). Convergence rates at each end of the trench are derived from the relative motion between the forearc blocks of the Hikurangi margin relative to the subducting Pacific Plate (Wallace et al., 2004a, 2009b).

B.12 Kermadec

Most of the values for the Kermadec Trench are taken from Power et al. (2011). The convergence rates at the Kermadec Trench are for the Kermadec Arc relative to the Pacific Plate, and are based on elastic block modelling of a GPS velocity from a site in the Kermadec Islands (Raoul Island) and earthquake slip vectors and transform orientations from events on the Kermadec Trench and in the Havre Trough (respectively) (Power et al., 2011). The preferred down-dip limit of rupture and the maximum coupling coefficient (0.8) are based on the depth of interseismic coupling on the megathrust in the Kermadec Islands (locking on the down to 30 km depth is required to fit GPS data from Raoul Island) (Power et al., 2011). We use a lower preferred coupling coefficient (0.3), given the possibility that the coupling observed from GPS data at Raoul Island is not representative of coupling on the Kermadec Trench elsewhere. The dip is based on the average dips of the interface estimated from seismic surveys of the Kermadec Trench (Scherwath et al., 2008). The minimum Mmax of 8.1 is based on the estimated magnitude of the largest historical event on the Kermadec Trench, occurring in May 1917 (see Power et al., 2011).

B.13 Tonga

The convergence rates we prescribe for the Tonga Trench reflect motion between the Tonga arc and the subducting Pacific plate; these are based on results from elastic block modelling of GPS velocities and earthquake slip vectors (Wallace et al., 2005). Despite the very high convergence rates at the Tonga Trench (up to 250 mm/yr) no earthquakes larger than Mw 8.0 have occurred here and abundant Mw 6.0-8.0 events have occurred on the subduction interface. Thus, we assign a relatively low preferred coupling coefficient to the Tonga Trench. The largest historical earthquake on the Tonga Trench was an Mw 8.0 in 2009 (Beavan et al., 2010b; Lay et al., 2010), so we use this as a minimum Mmax value, given that the historical record is short and it is likely that earthquakes larger than Mw 8.0 are possible.

B.14 Puysegur

The Mw 7.8 Dusky Sound earthquake in July 2009 is the largest subduction thrust event recorded at the Puysegur Trench. We base our preferred down-dip rupture limits on GPS observations that show slip down to 35 km depth in the event (Beavan et al., 2010). We use an upper limit on the rupture depth of 45 km, where postseismic slip was observed following the 2009 earthquake (Beavan et al., 2010a). For the minimum Mmax value, we assume Mw 7.8 based on the Dusky Sound earthquake. High interseismic coupling was observed on the Puysegur Trench in the region of the Dusky Sound earthquake prior to that event (Wallace et al., 2007), so we assume a relatively high coupling coefficient, but acknowledge that this has a large uncertainty due to the short historical record and the lack of geodetic coverage above much of the Puysegur subduction zone.

B.15 Hjort

Subduction of the Macquarie Plate beneath the Pacific Plate is accommodated at the Hjort Trench. Relative motion between the Macquarie Plate and the Pacific Plate is low, and we use the estimates of DeMets et al. (2010). Meckel et al. (2005) divide the trench into two portions: Northern Hjort (55.5°S-57.5°S) and Southern Hjort (57.5S-59.5S). Meckel et al. (2003) postulate a low angle oblique-slip fault at the Hjort Trench (between 55-58°S), dipping ~ 10°, at least down to 10 km (based on gravity data and seismic reflection data). Below 10 km, it is likely that the geometry of the fault steepens. At the southernmost part of the Hjort trench (59.5 deg S), Meckel et al. (2003) suggest that the Trench likely steepens (to ~45°). We assume 22°average dip to encompass this range of steep to shallow dip values. Meckel et al. (2003; 2005) suggest that there has only been a small amount of underthrusting of the Macquarie Plate, so we restrict the down-dip limit of any ruptures to ~20 km depth. Very little historical seismicity has been observed in the region of the Hjort Trench, with no events larger than Mw 7.2.

B.16 Northwest Solomon

This segment comprises the eastern end of the New Britain Trench adjacent to Bougainville, and north of the triple junction between the Woodlark, Pacific, and Australian Plates. Clusters of Mw 7.3-8.1 earthquakes have been observed in the northwest Solomons approximately every 30 years for the last century (Lay and Kanamori, 1980). More recently, the 2007 Mw 8.1 earthquake ruptured the southern half of this segment (as well as the northern part of the San Cristobal Trench, south of the triple junction.) We define a minimum Mmax of 8.1, consistent with historical seismicity. We use relatively high coupling coefficients for this subduction source (0.7 ± 0.1) based on the large (Mw >8.0) that occur along this trench on a relatively regular basis.

B.17 Southeast Solomon

This segment comprises the San Cristobal Trench, east of the triple junction between the Woodlark, Pacific, and Australian Plates. The eastern boundary of this source is where a 90° turn is taken in the orientation of the trench near Vanuatu. Overall, we use similar values for this subduction segment to those used for the northwest Solomons. Possibilities for simultaneous rupture across northwest and southeast Solomons segments must also be accounted for, as was observed to occur during the 2007 Mw 8.1 earthquake (Taylor et al., 2008a).

B.18 New Hebrides

The New Hebrides Trench is divided into four segments, northern, central, southern, and the Matthew-Hunter segment. Scenarios involving rupture across the first three segments should be considered. The relative motion at the New Hebrides trench is determined by elastic block modelling of GPS velocities and earthquake slip vectors (Power et al., 2011). The relative motion at the central and southern New Hebrides segments are the New Hebrides forearc/arc blocks relative to the subducting Australian Plate, while the relative motion at the Matthew-Hunter segment reflects the motion of the Matthew and Hunter Islands relative to the Australian Plate. The northern segment reflects motion between the Australian and Pacific Plates. GPS models of interseismic coupling suggest deep, high interseismic coupling along the northern New Hebrides segment, while interseismic coupling appears lower on the southern New Hebrides segment. The degree of interseismic coupling on the Matthew Hunter segment is not well-resolved. We use the down-dip limit of interseismic coupling on the central New Hebrides segment (Power et al., 2011) to define our preferred down-dip limit in that area. We make the down-dip limit on the southern and northern segment slightly shallower due to the lack of geodetic evidence for deep interseismic coupling. Much of the upper plate for the Matthew Hunter segment is recently rifted oceanic crust (related to north Fiji Basin development), so the depth to the down-dip limit of possible rupture is likely to be lower than for the north and south New Hebrides segments. Using subduction thrust events on the Matthew Hunter segment, Power et al. (2011) estimate a b-value of 0.74, which we use as the minimum value for this segment. The largest historical earthquake on the Matthew Hunter segment (in 1901) is estimated at Mw 8.4, although the data are somewhat ambiguous (see review in Power et al., 2011), so we use this for our preferred Mmax value and Mw 8.0 as our minimum Mmax value. The Mmax in a PSHA model developed for Vanuatu (Suckale and Grünthal, 2009) is Mw 8.3 for the northern segment, and Mw 7.6 for the southern segment. These Mmax values are based on historical data, so we adopt these as our minimum Mmax value. The slab is difficult to define in the Matthew Hunter segment due to the relatively lower level of seismicity there, so we adopt an average dip of 28° for the Matthew Hunter segment, following the slab geometry model developed by Power et al. (2011).

B.19 New Britain

We consider the western end of the New Britain Trench as the point where the Ramu Markham Fault goes offshore near Lae, Papua New Guinea. The eastern end is the cusp in the New Britain Trench where it bends strongly to the southeast near 153°E. Convergence rates at the New Britain Trench reflect motion of the Woodlark Plate relative to the South Bismarck Plate using poles of rotation from Wallace et al. (2004b). This subduction zone is very seismically active, with frequent moderate to large events. The largest historical subduction interface earthquakes that have occurred on the New Britain Trench have been Mw ~8.0 (e.g., Park and Mori, 2007), so we use this as our minimum Mmax estimate. Due to the occurrence of some subduction thrust events down to ~40 km depth (Park and Mori, 2007) we use this as the preferred down-dip limit of seismogenic zone. Due to the similarities in the level of seismicity and tectonic setting as the San Cristobal Trench offshore the Solomon Islands, we use the same coupling coefficients.

B.20 New Guinea

The eastern half of the New Guinea Trench accommodates southwest subduction of the Pacific, North Bismarck, and/or Caroline Plates (note that the motion of all three plates is very similar) beneath the north coast of the island of New Guinea. To determine the rate of convergence on the eastern half, we use the pole of rotation of the Pacific Plate relative to the New Guinea Highlands (NGH) plate from Wallace et al. (2004b). The relative motion in western half of the New Guinea Trench reflects motion between the Caroline Plate and the Bird's Head Block (e.g., Bird, 2003). We thus divide the New Guinea trench into two segments reflecting this. The largest historic event on the eastern part of the New Guinea Trench was Mw 7.6 in 2002 (Tregoning and Gorbatov, 2004), while the largest historic event on the western segment was the Biak earthquake in 1996 (Mw 8.2). The shallow geometry of the slab subducting at the New Guinea Trench is not well known. We assume a 30 km maximum down-dip limit for seismogenesis, and an average dip of 15°.

B.21 Manus (east and west)

The Manus trench accommodates very slow southward subduction of the Pacific and Caroline Plates beneath the north Bismarck Plate. Very little is known about the seismogenic potential of this feature, and whether or not it is truly a subduction zone. Thus, we largely use default values to parameterize this source. In absence of any major historical subduction thrust earthquakes on this trench, we assume a minimum Mmax of 7.5 here.

B.22 Andaman

We base many of our Andaman source parameters on geodetic and seismological studies of coseismic slip in the 2004 Mw 9.0-9.3 earthquake that ruptured along much of the Andaman Trench. The 2004 earthquake is the largest earthquake documented along the Andaman trench. We assign the northern and southern boundaries of this source coincide with the limits of rupture in the 2004 earthquake. We assume average dips (14°) and widths (~150 km), and depths (~40 km) of the source that are consistent with GPS studies of coseismic deformation in the earthquake (Subaraya et al., 2006). Based on the large tsunami produced in this event, we assume the updip limit of rupture to be within 2 km seafloor, with a maximum value of 5 km depth. We also assume a relatively high coupling coefficient, given the proven ability of this trench to produce large slip that helps to accommodate a major proportion of the plate motion budget.

B.23 Sumatra

Abundant seismological, paleoseismic and geodetic data (see reviews in Subaraya et al., 2006; McCaffrey, 2009; and Prawirodirdjo et al., 2010) exist to help constrain the source we use for the thrust accommodating subduction of the Indo-Australian Plate beneath Sumatra. The largest observed historical earthquake on this source segment was a Magnitude 9.0 in 1833, which we use as a minimum estimate for our Mmax. Depending on the geometry of the subduction thrust, maximum interseismic coupling depths (and we assume maximum rupture depths) are 25-50 km depth (Prawirodirdjo et al., 2010). Interseismic coupling values from geodetic studies are close to one, so we assume high interseismic coupling for this segment in this study.

B.24 Java

The largest historic subduction thrust events to occur at the Java Trench were the 1994 and 2006 Mw 7.8 earthquakes (Abercrombie et al., 2001; Ammon et al., 2006), the former caused a much larger tsunami than expected from its magnitude. The main slip in the 1994 earthquake occurred at ~20 km depth, which we assume as a minimum estimate for the down-dip limit of slip in earthquakes on this segment. We assume a slightly deeper depth (25 km) as our preferred down-dip limit estimate, and account for the possibility that even deeper rupture could occur (by assuming a maximum down-dip limit of 40 km). Much of the Java Trench is thought to be dominated by aseismic creep, rather than deep interesismic coupling (in contrast to Sumatra), so we assume a low coupling coefficient for this source. Fujii and Satake (2006) estimate very shallow propagation of the 2006 rupture, based on interpretation and modelling of tsunami observations from that event, justifying our choice of a shallow updip limit for the seismogenic zone.

B.25 Calabria

Most geometric and kinematic parameters of this source are drawn from the European Database of Seismogenic Faults (EDSF) (Basili et al., 2013a) and literature review by Basili et al. (2013b). According to GPS velocities and current plate models, relative motion between the subducting Africa plate and the European plate at the Calabria margin results in a convergence rate of 2-5 mm/y (D'Agostino and Selvaggi, 2004; Devoti et al., 2008; Serpelloni et al., 2010; D'Agostino et al., 2011). Very little is known about the seismogenic potential of the slab interface in the Calabrian arc. We largely use default seismic values for this source. However, there was a historic earthquake in 1905 with Mw 7.1, doubtfully associated with the subduction, which we take as the lower end of our Mmax range.

B.26 Hellenic

Most geometric and kinematic parameters of this source are drawn from the EDSF (Basili et al., 2013 a) and literature review by Basili et al. (2013b). According to GPS velocities and current plate models (e.g., Reilinger et al., 2006; Ganas and Parsons, 2009), in the western part of the arc relative motions result in a convergence rate of 35 mm/y. In the eastern part, where relative plate motion is oblique, the lateral component is of about 10 mm/y. GPS velocities of the Aegean plate progressively decrease toward the northwest, where the subduction zone approaches its lateral termination in the Ionian Islands (Hollenstein et al., 2008). Very little is known about the seismogenic potential of the Hellenic subduction zone from the instrumental period. Much controversy exists over whether or not this subduction thrust is dominated by aseismic creep (Reilinger et al., 2006; Shaw and Jackson, 2010) or if it has a very high coupling coefficient (Ganas and Parsons, 2009). Thus, we assume a broad range of possible coupling coefficients. Shaw and Jackson (2010) observe shallowly dipping thrust events on or near the interface between 15 km and 45 km depth, so we assume 45 km depth as our preferred down-dip limit of the seismogenic zone. Some studies suggest that a magnitude 8.4 earthquake that caused uplift at Crete in AD 365 occurred on the subduction interface (Ganas and Parsons, 2009), while others suggest that it was on an upper plate fault (Shaw and Jackson, 2010). If this event occurred on the subduction interface, the maximum rupture depth would have been 68 km, which we assume as a constraint for the down-dip limit of the seismogenic zone. We use the AD 365 possible subduction thrust event as our preferred Mmax. A magnitude 8.0 earthquake in eastern Crete in 1303 (Guidoboni and Comastri, 1997), could also be thought to represent rupture of the subduction interface. Also note the shallow portion of the Hellenic Trench dips at a very low angle.

B.27 Cyprus

Most geometric and kinematic parameters of this source are drawn from the EDSF (Basili et al., 2013a). According to GPS velocities and current plate models, relative motions result in an orthogonal convergence of about 18 mm/y (Reilinger et al., 2006) or 14 mm/y in the western part of the arc, decreasing eastwards to 7-9 mm/y, where relative motion becomes oblique (Wdowinski et al., 2006). The Paphos Fault is thought to accommodate about 10 mm/y of differential velocity between the eastern and western segments of the arc. Little is known about the subduction thrust earthquake potential of the Cyprus Arc, so we largely use default seismic values here. However, the largest historic earthquakes in the Cyprus area thought to have occurred on the subduction thrust are the 342 AD and 1222. Magnitude estimates vary a lot for both, Mw 6.6 to 7.4 for the first one (Guidoboni et al., 2007; Cagnan and Tanircan, 2010) and Mw 6 to 7.5 for the second (Guidoboni et al., 2007; Guidoboni and Comastri, 2005; Yolsal et al., 2007). We use the largest (Mw=7.5) of these estimates as our minimum value for Mmax.

B.28 Makran

The largest subduction thrust event on the Makran Trench was an Mw 8.1 in 1945 that triggered a large tsunami, killing up to 4000 people (Heidarzadeh et al., 2008). Vernant et al. (2004) show from GPS measurements that convergence rates at the Makran Trench are 19.5 ± 2 mm/yr. Seismic reflection profiles across the Makran Trench show a dip angle between 2 and 8° (Koppa et al., 2000; Schluter et al., 2002), so we assume an average dip of 8°, which is at the upper end of this range to also account for the possibility that the slab steepens up with depth (beyond the range of seismic reflection imaging). The Makran system has a very thick incoming sedimentary package (up to 7 km thick; Koppa et al., 2000), and the trench is not well-defined morphologically (Schluter et al., 2002), so we assume a somewhat deeper updip limit of seismogenic rupture compared to other places. Following the overview of historical seismicity at Makran in Heidarzadeh et al. (2008), we assume 35 km as a preferred down-dip limit of the seismogenic zone.

B.29 Ecuador/Columbia segment of the Andean margin

The largest historical earthquake in this segment was an Mw 8.8 in 1906 (see review in Bilek, 2010). We assume relatively high coupling coefficients for all of the Andean margin segments, due to the seismically productive nature of this subduction system.

B.30 Peru segment of the Andean margin

The largest historical earthquake in this segment was an Mw 8.4 in 2004 (see review in Bilek, 2010).

B.31 Northern Chile segment of the Andean margin

The largest historical earthquake in this segment was an Mw 8.6 in 1906 (see review in Bilek, 2010).

B.32 Central Chile segment of the Andean margin

The largest historical earthquake in this segment was an Mw 9.5 in 1960 (see review in Bilek, 2010; Cifuentes and Silver, 1989). Using the length limited approach to assessing the maximum possible Mmax, we also calculate 9.5.

B.33 Patagonia (north and south segments)

The convergence rates at the far southern end of the Chile Trench are much slower (10-20 mm/yr) compared to further north. No significant historical seismicity has occurred on this segment of the Chile Trench. This may be due to the low convergence rates in the segment of the subduction zone, and we cannot rule out the possibility that large subduction thrust earthquakes occur here. Due to our lack of knowledge about the behavior of the subduction thrust in this portion of the Andean margin, we largely use default values and assume a minimum Mmax of 8.0.

B.34 South Shetland Islands

Very little is known about historical seismicity at this subduction zone. Convergence rates are very low at this trench (<10 mm/yr; Taylor et al., 2008b), so the historical record is not likely to be representative of the seismogenic potential of this subduction margin. Due to our lack of knowledge about the behaviour of this subduction zone, we largely assign default values.

B.35 South Sandwich

Very little is known about the potential for large subduction thrust earthquakes subduction zone. Convergence rates are reasonably high (70-90 mm/yr) and historical subduction thrust earthquakes larger than Mw 7.0 have rarely been observed here, leading some to suggest that subduction here is largely aseismic (Frankel and McCann, 1979). The exception is the far southern end of the trench (south of 59°S), where earthquakes up to Mw 7.4 have been observed (Frankel and McCann, 1979). Based on this, we assign a low preferred coupling coefficient (0.2 ± 0.1) to this subduction source. Due to our lack of knowledge about the behaviour of this subduction zone, we largely assign default values to the other parameters.

B.36 Jalisco segment of Middle America

The largest historic subduction thrust event to rupture this portion of the Middle America Trench was the 1932 Mw 8.2 earthquake. More recently, an Mw 8.0 earthquake occurred on this segment of the Middle America Trench in 1995. Slip in the 1995 earthquake was largely focused shallower than 20 km depth, so we assume 25 km depth as our maximum down-dip limit of rupture. Interpretation of GPS velocities from the Jalisco region can fit the data assuming 50% coupling coefficient on the Middle America Trench (Selvans et al., 2010), so we assume 0.5 ± 0.2 for our coupling coefficient.

B.37 Michoacan to Guatemala portion of Middle America

A well-documented array of historical subduction thrust earthquakes have occurred on this portion of the Middle America Trench. Based on the distribution of those events (see overview of previous studies in

Pacheco and Singh, 2010) as well as observations of interseismic coupling and slow slip events in the Oaxaca and Guerrero regions, we assign a preferred down-dip limit of coupling as 25 ± 5 km. The largest historic earthquake on this segment was an Mw 8.0 in 1985. In general, the down-dip limit of rupture in these historical earthquakes is ~25 km, and slow slip event behaviour appears to occur down to ~35-40 km depth (Larson et al., 2004). Due to the high seismic productivity of this portion of the Middle American Trench, and high interseismic coupling estimates from campaign GPS (Larson et al., 2004) we assume a coupling coefficient of 0.7 ± 0.2.

B.38 Middle America – El Salvador to Nicaragua

This portion of the Middle America Trench frequently experiences moderate sized subduction thrust earthquakes (Mw 6.0-7.4), but rarely experiences really large earthquakes. The 2 September 1992 (Mw 7.6) Nicaragua tsunami earthquake established the potential for shallow rupture to the trench. There is a suspected M 8 subduction thrust event in 1915 (Ambraseys and Adams, 2001). GPS data suggest that if interseismic coupling occurs on this portion of the Middle America Trench it must be shallow (<20 km depth, La Femina et al., 2009) and that the coupling ratio is likely to be low. Thus, we assume a down-dip limit to the seismogenic zone of 20±5, and 0.3 for the preferred coupling coefficient.

B.39 Middle America – Costa Rica to west Panama

This segment of the Middle America Trench produces Mw 6-7.5 earthquakes on a regular basis, approximately every decade or so. The largest historic subduction thrust event on this portion of the trench was a Mw 7.7 earthquake beneath the Nicoya Peninsula in 1950. GPS studies of interseismic coupling (Norabuena et al., 2004; LaFemina et al., 2009) on the Middle America Trench suggest interseismic locking down to 20 km depth, and possibly deeper in some places. LaFemina et al. (2009) obtain an average interseismic coupling coefficient of 0.5.

B.40 Lesser Antilles

Subduction of North America beneath the Caribbean Plate occurs at the Antilles Trench. Little is known about the seismogenic potential of this feature, and the largest historic subduction thrust event is the 1843 Magnitude 7.5-8.0 earthquake at the northern end of the trench (Bernard and Lambert, 1988). Virtually nothing else is known about the seismogenic zone geometry and potential for subduction earthquake occurrence at this subduction zone, so we largely use default values for this source.

B.41 Manila

Galgana et al. (2007) use GPS to estimate low interseismic coupling (near zero) on the Manila Trench, so we assume a coupling coefficient of 0.15 ± 0.1. Results of Beavan et al. (2001) also suggest largely aseismic deformation on the Manila Trench. Although data on historic subduction interface earthquakes at the Manila Trench is sparse, Hamburger et al. (1983) noted two large earthquakes in 1934 and 1948 (magnitudes 7.6 and 7.2, respectively), which they suggest could represent interplate thrust events. Given the lack of significant historic subduction thrust seismicity on the Manila Trench, we know very little about the depth to the down-dip limit of the seismogenic zone, and other relevant parameters, so we largely use default values for these.

B.42 Philippine

We use the motion of the southeast Luzon block relative to the Philippine Sea Plate from Galgana et al. (2007) to determine the rate and azimuth of convergence on the Philippine Trench. The largest historic event on the Philippine Trench was the 1907 M 7.0-7.6 earthquake (Hamburger et al., 1983). Little is known about the earthquake potential of the Philippine Trench, and published GPS studies in the region of the Philippine Trench are sparse. However Galgana et al. (2007) see some evidence for elastic strain accumulation on the northern end of the Philippine Trench and estimate a coupling coefficient of 0.27.

B.43 East Luzon

The east Luzon Trough is the northward continuation of the Philippine Trench, and is thought to be accommodating incipient subduction of the Philippine Sea Plate (Hamburger et al., 1983). Galgana et al. (2007) estimate 9-15 mm/yr of convergence at the southern end of this feature. To calculate the rates of motion on this feature we use the pole of rotation for northeastern Luzon relative to the Pacific Plate from Galgana et al. (2007). The Luzon Trough seismogenic potential is not well-understood, although there are a number of historic events with underthrusting focal mechanisms (Hamburger et al., 1983). Seismicity defines a 20° dipping plate down to ~50 km depth (Hamburger et al., 1983). The largest historical earthquake thought to be associated with the Luzon Trough was a magnitude 7.3 in 1968 (Hamburger et al., 1983). Due to our lack of understanding of the Luzon Trough as a subduction earthquake source we use default values for the other parameters defining this feature.

B.44 Cotabato

This inferred subduction zone accommodates subduction of the Celebes Sea crust beneath southwest Mindanao, and has generated major earthquakes and tsunami over the last 40 years. The largest historic event on this feature was the 1976 Mw 8.0 Moro Gulf earthquake, which caused a devastating tsunami in the region. Although GPS coverage in the southern Philippines is sparse, we use the pole of rotation for Mindanao relative to Sunda calculated by Galgana et al. (2007) to estimate convergence rates at the Cotabato Trench. For most of the other parameters, we assume default values due to our lack of detailed knowledge about this feature. We assume a dip of 15° for the subduction thrust, based on typical dips for similar subduction zones.

B.45 Sulu

This inferred subduction zone accommodates subduction of the Sulu Basin beneath western Mindanao, and is thought to have generated a major subduction thrust event in 1897 (magnitude ~8.0). Although GPS coverage in the southern Philippines is sparse, we use the pole of rotation for Mindanao relative to Sunda calculated by Galgana et al. (2007) to estimate convergence rates at the Sulu Trench. For most of the other parameters, we assume default values due to our lack of detailed knowledge about this feature. We assume a dip of 15° for the subduction thrust, based on typical dips for similar subduction zones.

B.46 Minahassa

The Minahassa Trench along the north coast of Sulawesi accommodates subduction of the Celebes Basin beneath the northern arm of Sulawesi. This feature produces significant subduction thrust earthquakes; the largest historic event was an Mw 7.9 earthquake in 1996, which was followed by an eastward propagating sequence of moderate to large subduction thrust events over the following year or two (Vigny et al., 2002). To estimate convergence rates at the western end of the Minahassa Trench we use Socquet et al.'s (2006) pole of rotation for the Sunda block relative to the north Sula block. For the eastern end of the Trench we use Socquet et al.'s (2006) pole for the Manado block relative to the Sunda block. We assume an average dip of 15° for the subduction thrust, based on typical dips for similar subduction zones.

B.47 Seram

The largest historic earthquake in the region was an Mw 8.5 earthquake in 1938. Okal and Reymond (2003) suggest a thrust mechanism at ~60 km depth. Although Okal and Reymond (2003) suggest that the earthquake was either within the subducting slab, or within the mantle wedge (due to its depth and the fact that it is ~100 km from the Seram Trough), we consider the possibility that this event occurred along the deeper part of the seismogenic zone on the plate interface, so assume this as our preferred Mmax, with a minimum Mmax of 8.0. Very little else is known about the subduction thrust earthquake potential of the Seram Trough, so we largely use default values.

B.48 Timor

The Timor Trough is thought to have recently ceased activity due to the impingement of the Australian continental margin, with most of the relative plate motion transferred onto reverse faults in the back-arc, such as the Wetar and Flores thrusts. It is not known if this continues to accommodate active tectonic motion. The historical seismicity on the Timor Trough is very sparse. Due to our lack of knowledge about the seismogenic potential of the plate interface at the Timor Trough, we largely assign default values, and assume Mw 8.0 for preferred Mmax, with Mw 7.5 as a minimum Mmax.

B.49 Manokwari

The largest historic underthrusting earthquake at the Manokwari Trench was a Mw 7.6 on 3 January 2009. Very little else is known about the subduction thrust earthquake potential of the Manokwari Trench, so we largely use default values.

B.50 Molucca Sea

The largest historic event in this region was the 14 May 1932 magnitude 8.3. Beyond that, we know very little about the seismogenic potential of this complex region, and resort to default values to parameterize these sources.